



Spatial–temporal patterns of inorganic nitrogen air concentrations and deposition in eastern China

Wen Xu^{1,2}, Lei Liu³, Miaomiao Cheng⁴, Yuanhong Zhao⁵, Lin Zhang⁵, Yuepeng Pan⁶, Xiuming Zhang⁷, Baojing Gu⁸, Yi Li⁹, Xiuying Zhang³, Jianlin Shen¹⁰, Li Lu¹¹, Xiaosheng Luo¹², Yu Zhao¹³, Zhaozhong Feng², Jeffrey L. Collett Jr.¹⁴, Fusuo Zhang¹, and Xuejun Liu¹

¹College of Resources and Environmental Sciences, Key Laboratory of Plant-Soil Interactions of MOE, Beijing Key Laboratory of Cropland Pollution Control and Remediation, China Agricultural University, Beijing 100193, China

²State Key Laboratory of Urban and Regional Ecology, Research Center for Eco-Environmental Sciences, Chinese Academy of Sciences, Shuangqing Road 18, Haidian District, Beijing 100085, China

³Jiangsu Provincial Key Laboratory of Geographic Information Science and Technology, International Institute for Earth System Science, Nanjing University, Nanjing 210023, China

⁴State Key Laboratory of Environmental Criteria and Risk Assessment, Chinese Research Academy of Environmental Sciences, Beijing 100012, China

⁵Laboratory for Climate and Ocean-Atmosphere Sciences, Department of Atmospheric and Oceanic Sciences, School of Physics, Peking University, Beijing 100871, China

⁶State Key Laboratory of Atmospheric Boundary Layer Physics and Atmospheric Chemistry (LAPC), Institute of Atmospheric Physics, Chinese Academy of Sciences, Beijing 100029, China

⁷School of Agriculture and Food Sciences, The University of Melbourne, Victoria, 3010, Australia

⁸Department of Land Management, Zhejiang University, Hangzhou 310058, China

⁹Arizona Department of Environmental Quality, Phoenix, AZ 85007, USA

¹⁰Institute of Subtropical Agriculture, Chinese Academy of Sciences, Changsha 410125, China

¹¹Institute of Surface-Earth System Science, Tianjin University, Tianjin 300072, China

¹²Institute of Plant Nutrition, Resources and Environmental Sciences, Henan Academy of Agricultural Sciences, Henan Key Laboratory of Agricultural Eco-environment, Zhengzhou 450002, China

¹³State Key Laboratory of Pollution Control & Resource Reuse, School of the Environment, Nanjing University, 163 Xianlin Ave., Nanjing, Jiangsu 210023, China

¹⁴Department of Atmospheric Science, Colorado State University, Fort Collins, Colorado, 80523 USA

Correspondence: Xuejun Liu (liu310@cau.edu.cn) and Zhaozhong Feng (fzz@rcees.ac.cn)

Received: 26 April 2018 – Discussion started: 15 May 2018

Revised: 11 July 2018 – Accepted: 17 July 2018 – Published: 6 August 2018

Abstract. Five-year (2011–2015) measurements of gaseous NH_3 , NO_2 , and HNO_3 and particulate NH_4^+ and NO_3^- in air and/or precipitation were conducted at 27 sites in the Nationwide Nitrogen Deposition Monitoring Network (NNDMN) to better understand spatial and temporal (seasonal and annual) characteristics of reactive nitrogen (N_r) concentrations and deposition in eastern China. Our observations reveal annual average concentrations ($16.4\text{--}32.6\ \mu\text{g N m}^{-3}$), dry deposition fluxes ($15.8\text{--}31.7\ \text{kg N ha}^{-1}\ \text{yr}^{-1}$), and wet/bulk deposition fluxes ($18.4\text{--}28.0\ \text{kg N ha}^{-1}\ \text{yr}^{-1}$) based on land use,

ranked as urban > rural > background sites. Annual concentrations and dry deposition fluxes of each N_r species in air were comparable at urban and background sites in northern and southern regions, but were significantly higher at northern rural sites. These results, together with good agreement between spatial distributions of NH_3 and NO_2 concentrations determined from ground measurements and satellite observations, demonstrate that atmospheric N_r pollution is heavier in the northern region than in the southern region. No significant inter-annual trends were found in the annual N_r dry

and wet/bulk N deposition at almost all of the selected sites. A lack of significant changes in annual averages between the 2013–2015 and 2011–2012 periods for all land use types suggests that any effects of current emission controls are not yet apparent in N_r pollution and deposition in the region. Ambient concentrations of total N_r exhibited non-significant seasonal variation at all land use types, although significant seasonal variations were found for individual N_r species (e.g. NH_3 , NO_2 , and pNO_3^-) in most cases. In contrast, dry deposition of total N_r exhibited a consistent and significant seasonal variation at all land use types, with the highest fluxes in summer and the lowest in winter. Based on sensitivity tests by the GEOS-Chem model, we found that NH_3 emissions from fertilizer use (including chemical and organic fertilizers) were the largest contributor (36 %) to total inorganic N_r deposition over eastern China. Our results not only improve the understanding of spatial–temporal variations of N_r concentrations and deposition in this pollution hotspot, but also provide useful information for policy-makers that mitigation of NH_3 emissions should be a priority to tackle serious N deposition in eastern China.

1 Introduction

In China, and globally, human activities have dramatically increased emissions of nitrogen oxides ($NO_x = NO + NO_2$) and ammonia (NH_3) into the atmosphere since the beginning of the industrial revolution (Galloway et al., 2008; Liu et al., 2013). NO_x and NH_3 emitted into the atmosphere are transformed to nitrogen-containing particles (e.g. particulate NH_4^+ and NO_3^- , and organic nitrogen; Ianniello et al., 2010; Zhang et al., 2015), which are major chemical constituents of airborne $PM_{2.5}$ (particulate matter with a diameter of 2.5 μm or less) and have implications for air quality and climate (Fuzzi et al., 2015). As a result of elevated reactive nitrogen (N_r) emissions, nitrogen (N) deposition through dry and wet processes has also substantially increased over China (Liu et al., 2013; Lu et al., 2007, 2014; Jia et al., 2014, 2016), and excessive deposition of N has resulted in detrimental impacts including decreased biological diversity (Bobbink et al., 2010), nutrient imbalance (Li et al., 2016), increased soil acidification (Yang et al., 2015), and eutrophication of water bodies (Fenn et al., 2003). Furthermore, N_r -associated haze pollution episodes, characterized by high concentrations of $PM_{2.5}$, occur frequently in China, as evidenced in particular in 2013 (Guo et al., 2014; Huang et al., 2014; Tian et al., 2014).

In order to control its notorious air pollution, China has reduced national emissions of SO_2 and particulate matter by 14 and 30 % respectively from 2005 to 2010 (MEPC, 2011). Additionally, stringent measures (e.g. using selective catalytic/non-catalytic reduction systems, and implementing tighter vehicle emission standards) were implemented during the 12th Five Year Plan (FYP) period (2011–2015), with

aims to reduce 2015 annual emissions of SO_2 and NO_x by 8 and 10 % respectively relative to 2010 levels (Xia et al., 2016). However, there is as yet no regulation or legislation that deals with national NH_3 emissions and thus the emission reductions of SO_2 and NO_x used to achieve desired air-quality improvement goals will be compromised (Gu et al., 2014). Significant increases in $PM_{2.5}$ concentrations have been observed in the years 2013 and 2014 as compared to 2012, excluding the influence of meteorological conditions on inter-annual variations (Liang et al., 2015). Other studies with more conclusive evidence have likewise suggested that NH_3 plays a vital role in sulfate formation and exacerbates severe haze pollution development in urban regions of China (Wang et al., 2016), even acting as the key limiting factor for the formation of secondary inorganic aerosol (Wu et al., 2016). In addition, due to higher local and regional concentrations of NH_3 in the atmosphere, nitrate-driven haze pollution occurred during summertime in urban environment in the North China Plain (Li et al., 2018). The absolute and relative concentrations of particulate nitrate in urban Beijing increased with haze development (Pan et al., 2016). Also, nitrate contributed to a large fraction of the elevated $PM_{2.5}$ concentrations at a rural site in the North China Plain and high NH_3 in the early morning accelerated the formation of fine nitrates (Wen et al., 2015).

High rates of N deposition have also been observed during 2011–2014 across China (Xu et al., 2015). However, to date, no study based on long-term ground-based observations has provided any information on the effectiveness of SO_2 and NO_x emission controls on N deposition in China. Non-linearities have been identified between reductions in emissions and deposition in Europe over the last 3 decades (Aguillaume et al., 2016; Fowler et al., 2007). Due to the tightly coupled yet complex relationship between emissions, concentrations, and deposition, long-term monitoring networks can test the effectiveness of emission controls (Erisman et al., 2003). Currently two national N deposition networks are operational in China, i.e. the Nationwide Nitrogen Deposition Monitoring Network (NNDMN, Liu et al., 2011; Xu et al., 2015) and the Chinese Ecosystem Research Network (CERS, Zhu et al., 2015). The NNDMN, containing 43 in situ monitoring sites, has been measuring wet N deposition and ambient concentrations of five major N_r species (i.e. gaseous NH_3 , NO_2 , and HNO_3 , and particulate NH_4^+ and NO_3^-) since 2010, the latter species for subsequent estimation of dry deposition. The CERS was established in 1988 and has been mainly focused on wet N deposition at 41 field stations. In addition to ground-based measurements, satellite observations enable retrieval of atmospheric NH_3 and NO_2 with high temporal and spatial resolutions (Dammer et al., 2016; Russell et al., 2012), providing a means to reveal spatial distributions and long-term trends of ambient NH_3 and NO_2 levels at regional to global scales, and also to evaluate the effectiveness of emission controls (Krotkov et al., 2016). However, to effectively use the vast satellite data sets for en-

vironmental monitoring, it is critical to validate these remote sensing observations using in situ surface observations (Pinder et al., 2011; Van Damme et al., 2015).

Eastern China is a developed region with the largest densities of population, economic activity, and resource consumption in the country (He et al., 2015). Recent satellite observations indicate that tropospheric NH_3 and NO_2 levels in eastern China were both much greater than other regions of the world over 2005–2015 (Demmer et al., 2016; Krotkov et al., 2016). Accordingly, this region received the highest levels of dry N deposition in the world (Vet et al., 2014), and was regarded as a primary export region of N deposition to neighbouring countries (Ge et al., 2014). Based on meta-analysis of published observations, some studies have provided information on the magnitudes, spatial distributions, and decadal variations of wet/bulk N deposition in China (Liu et al., 2013; Jia et al., 2014), but the analysed data were limited to time periods between 1980 and 2010. Although a recent study (Jia et al., 2016) has reported a clear increasing trend of dry N deposition in eastern China between 2005 and 2014, considerable uncertainty may exist due to estimates of gaseous HNO_3 and particulate NH_4^+ and NO_3^- ($p\text{NH}_4^+$ and $p\text{NO}_3^-$) concentrations using NO_2 satellite data, which is in part manifested in Liu et al. (2017a). Furthermore, seasonal patterns of N_r concentrations and deposition have not yet been systematically investigated at a large spatial scale in this region, although spatial patterns of dry N_r deposition for representative months of four seasons (i.e. January for winter, April for spring, July for summer, October for autumn) in 2010 have been mapped with the RAMS-CMAQ model (Han et al., 2017). Thus, the spatial and temporal (annual and seasonal) variations of N_r concentrations and dry and wet deposition in eastern China require further exploration using ground-based measurements, especially for time periods after 2010. Our previous work (Xu et al., 2015) used multi-year measurements (mainly from January 2010 to September 2014) at the 43 sites in the NNDMN, aiming to provide the first quantitative information on atmospheric N_r concentrations and pollution status across China, and to analyse overall fluxes and spatial variations of N_r deposition in relation to anthropogenic N_r emissions from six regions.

The present study aims to examine spatial–temporal (annual and seasonal) characteristics of N_r concentrations in air (NH_3 , NO_2 , HNO_3 , $p\text{NH}_4^+$, and $p\text{NO}_3^-$) and precipitation ($\text{NH}_4^+\text{-N}$ and $\text{NO}_3^-\text{-N}$), and their corresponding dry and wet/bulk N deposition, through a 5-year (2011–2015) monitoring period at 27 NNDMN sites in eastern China. In addition, we compare spatial–temporal variability of measured NH_3 and NO_2 concentrations with variations of the corresponding satellite retrieval columns, as well as inter-annual trends in N_r deposition and emissions. Finally, emission sources contributing to total N deposition over eastern China are examined.

2 Materials and methods

2.1 Study area and site descriptions

The present study was conducted in eastern China, which is distinguished by the “Hu Line” (She, 1998). This region has spatial heterogeneity in levels of economic development, and significant spatial differences in NH_3 and NO_x emissions (Fig. 1b and c). Thus, to better analyse spatial and temporal variabilities in measured N_r concentrations and deposition, we divided eastern China into northern and southern regions using the Qinling Mountains–Huaihe River line (Fig. 1a), the division basin of which was based on the differences in natural conditions, agricultural production, geographical features, and lifestyle. As for specific differentiations, for example, the northern region adopted a centralized domestic heating policy for late autumn and winter seasons but the south has not; annual average precipitation amounts were generally greater than 800 mm in the south but were less than 800 mm in the north. In addition, the north is dominated by calcareous soils, which could result in higher soil NH_3 volatilization (Huang et al., 2015), vs. the acidic red soil in the south.

The NNDMN was operated in line with international standards by China Agricultural University (CAU); 35 NNDMN sites were located in eastern China (Xu et al., 2015). For our analysis, we considered 27 sites in total, with 5-year continuous data: 13 sites were located in north of the Qinling Mountains–Huaihe River line (China Agricultural University: CAU, Zhengzhou: ZZ, Dalian: DL, Shangzhuang: SZ, Quzhou: QZ, Yangqu: YQ, Zhumadian: ZMD, Yanglin: YL, Yucheng: YC, Gongzhuling: GZL, Lishu: LS, Lingshanda: LSD, Changdao: CD), and 14 sites were located in south of the line (Nanjing: NJ, Baiyun: BY, Wenjiang: WJ, Wuxue: WX, Taojing: TJ, Fengyang: FYA, Zhanjiang: ZJ, Fuzhou: FZ, Fenghua: FH, Ziyang: ZY, Yangting: YT, Jiangjin: JJ, Huinong: HN, Xishan: XS).

All the sites are located as far away as possible and practical from local direct emission sources to increase regional representativeness. They can be divided into three categories according to their geopolitical location and their proximity to the main emission sources: urban sites (abbreviated as U), rural sites (cropland areas, R), and background sites (coastal and forest areas, B). Information on the monitoring sites, such as land use types, coordinates, and measurement periods are listed in Table S1 of the Supplement. Detailed descriptions of all the sites including the surrounding environment and nearby emission sources can be found in Xu et al. (2015).

2.2 Field sampling and chemical analysis

Continuous measurements were performed during the period from January 2011 to December 2015 at the 27 study sites, except for 11 sites (ZZ, ZMD, YC, LSD, NJ, WX, FYA, ZJ, YT, JJ, and HN), where field sampling was carried out after the year 2011 (i.e. the years between 2012 and 2015)

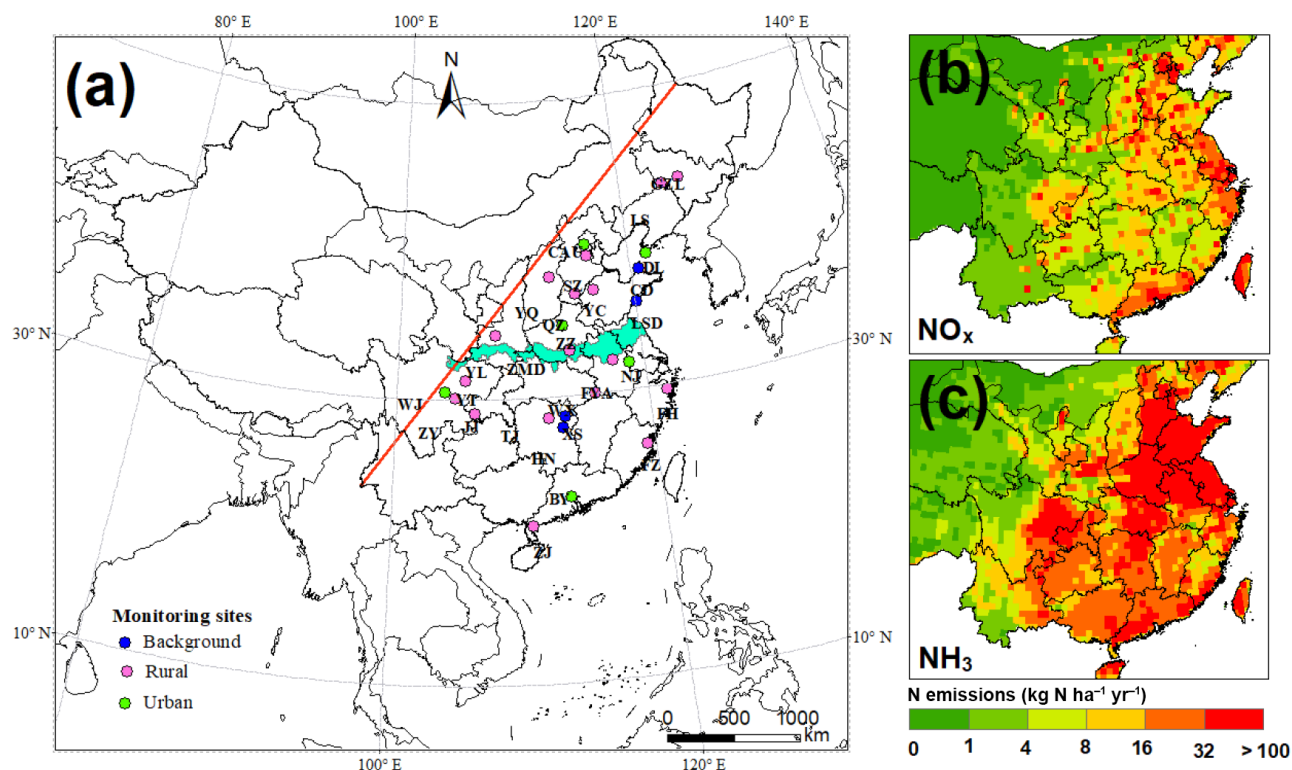


Figure 1. Spatial distributions of the 27 monitoring sites (a), NO_x emissions (b), and NH_3 emissions (c) in eastern China (NH_3 and NO_x emission data were for the year 2010 and obtained from Liu et al., 2017b). The blue and red lines refer to the Qinling–Huaihe line, and Hu line respectively.

and/or interrupted during the period due to instrument failure (details in Table S1, Supplement). Ambient N_r concentrations of gaseous NH_3 and HNO_3 , and $p\text{NH}_4^+$ and $p\text{NO}_3^-$ (for which the empirically determined effective size cut-off for aerosol sampling is of the order of $4.5\ \mu\text{m}$), were measured using an active DELTA (DENuder for Long-Term Atmospheric sampling; Tang et al., 2009) system; gaseous NO_2 was sampled in three replicates with passive diffusion tubes (Gradko International Limited, UK). The air intakes of the DELTA system and the NO_2 tubes were mounted 2 m above the ground at most sites and protected from precipitation and direct sunlight with a rigid plastic box and a PVC shelter respectively. All measurements of N_r concentration were based on monthly sampling (one sample per month for each N_r species). Detailed information on measuring methods and collection are given in Sect. S1 of the Supplement.

To collect precipitation (here termed as wet/bulk deposition, which contains wet and some dry deposition due to the use of an open sampler) samples, a standard precipitation gauge (SDM6, Tianjin Weather Equipment Inc., China) was continuously exposed beside the DELTA system ($\sim 2\ \text{m}$). Immediately after each precipitation event (08:00–08:00 the following day, Greenwich Mean Time +8), samples (including rain and melted snow) were collected and stored in clean polyethylene bottles (50 mL) at $-18\ ^\circ\text{C}$ until sent to the CAU

laboratory for analysis. Each collector was rinsed three times with high-purity water after each collection.

In the analytical laboratory, acid-coated denuders and aerosol filters were extracted with 6 and 10 mL of high-purity water ($18.2\ \text{M}\Omega$) respectively and analysed for $\text{NH}_4^+\text{-N}$ with an AA3 continuous-flow analyser (CFA; BranC Luebbe GmbH, Norderstedt, Germany). Carbonate-coated denuders and filters were both extracted with 10 mL 0.05 % H_2O_2 solution followed by analysis of $\text{NO}_3^-\text{-N}$ using the same CFA. NO_2 samples, extracted with a solution containing sulfanilamide, H_3PO_4 , and N-1-naphthylethylene-diamine, were determined using a colorimetric method by absorption at a wavelength of 542 nm (Xu et al., 2016). Precipitation samples were filtered through a syringe filter ($0.45\ \mu\text{m}$; Tengda Inc., Tianjin, China) and analysed for $\text{NH}_4^+\text{-N}$ and $\text{NO}_3^-\text{-N}$ using the CFA as mentioned above. Quality assurance and quality control procedures adopted in the analytical laboratory are described by Xu et al. (2017). Further details of precipitation measurement, samples handling, and chemical analysis are reported in Xu et al. (2015).

2.3 Deposition estimate

Wet/bulk deposition of $\text{NH}_4^+\text{-N}$ and $\text{NO}_3^-\text{-N}$ were calculated per month and year by multiplying the precipitation amount

by their respective volume-weighted mean (VWM) concentrations. The dry deposition flux of gaseous and particulate N_r species was calculated as the product of measured concentrations by modelled deposition velocities (V_d). The dry deposition velocities of five N_r species were calculated by the GEOS (Goddard Earth Observing System)-Chem chemical transport model (CTM; Bey et al., 2001; <http://geos-chem.org>), and have been reported in a companion paper (Xu et al., 2015). In brief, the model calculation of dry deposition of N_r species follows a standard big-leaf resistance-in-series model as described by Wesely (1989) for gases and Zhang et al. (2001) for aerosol. We used archived hourly V_d from January 2011 to May 2013 and filled the gap for the period (from June 2013 to December 2015) when GEOS meteorological data are unavailable using the mean values calculated from all the available simulations. The monthly V_d at each site was averaged from the hourly data set.

2.4 Satellite retrievals of NH_3 and NO_2

Comparisons between satellite observations and ground-based measurements were evaluated at the 27 sites in order to accurately examine the spatial–temporal pattern of NH_3 and NO_2 concentrations. For NH_3 , we used the products retrieved from the Infrared Atmospheric Sounding Interferometer (IASI) instrument (aboard the MetOp-A platform), which crosses the equator at a mean local solar time of 09:30 and 21:30. The IASI- NH_3 product is based on the calculation of a spectral hyperspectral range index and subsequent conversion to NH_3 total columns via a neural network. The details of the IASI- NH_3 retrieval method are described in Whitburn et al. (2016). We only considered the observations from the morning overpass as they are generally more sensitive to NH_3 because of higher thermal contrast at this time of day (Van Damme et al., 2015; Dammers et al., 2016). The daily IASI- NH_3 data (provided by the Atmospheric Spectroscopy Group at Université Libre De Bruxelles; data available at <http://iasi.aeris-data.fr/NH3/>) from 1 January 2011 to 31 December 2015 was used for the spatial analysis in the present study. For the temporal analysis, we used the IASI- NH_3 from 1 January 2011 to 30 September 2014 because an update of the input meteorological data on 30 September 2014 had caused a substantial increase in the retrieved atmospheric NH_3 columns. Only observations with a cloud coverage lower than 25 % and relative error lower than 100 %, or absolute error smaller than 5×10^{15} molecules cm^{-2} , were processed. The methodology is provided in detail in Liu et al. (2017b). In brief, all observations were gridded to a 0.5° latitude \times 0.5° longitude grid, and then we calculated the monthly arithmetic mean by averaging the daily values with observations points within each grid cell. Similarly, we calculated the annual arithmetic mean by averaging the daily values with observations points within the grid cell over the whole year.

For NO_2 we used the products from the Ozone Monitoring Instrument (OMI) onboard NASA's EOS-Aura satellite, which was launched in July 2004 into a sun-synchronous orbit with a local equator crossing time at approximately 13:45. OMI detects the backscattered solar radiation from the Earth's atmosphere within the UV–Vis spectral window between 270 and 500 nm, to achieve nearly global coverage daily, with a spatial resolution ranging from $13 \text{ km} \times 24 \text{ km}$ at nadir to $24 \text{ km} \times 128 \text{ km}$ at the edge of the swath (Russell et al., 2012). We used tropospheric NO_2 retrievals from the DOMINO (Dutch–Finnish Ozone Monitoring Instrument) algorithm version 2. The retrieval algorithm is described in detail in Boersma et al. (2007). The tropospheric NO_2 columns used in this study are monthly means from 1 January 2011 to 30 December 2015 with a spatial resolution of 0.125° latitude \times 0.125° longitude (data available at <http://www.temis.nl/airpollution/no2.html>).

2.5 Statistical analysis

One-way analysis of variance (ANOVA) and two independent samples t tests were applied to detect significant differences in seasonal mean concentrations and deposition fluxes of measured N_r species as well as their annual mean deposition fluxes for three land use types (rural, urban, and background). As there was large site-to-site variability in annual N_r concentrations and deposition fluxes at monitoring sites within the same land use types, averaging data into annual values for land use types is unlikely to be truly representative of actual trends. Thus, annual trends of the variables were evaluated at a single site scale rather than by land use type. Trend analysis was conducted using Theil regression (Theil, 1992) and the Mann–Kendall test (Gilbert, 1987; Marchetto et al., 2013). We defined an increasing (decreasing) trend as a positive (negative) slope of the Theil regression, while a statistical significance level ($p < 0.01$) of a trend was evaluated by the non-parametric Mann–Kendall test (p value). Non-parametric methods usually have the advantage of being insensitive to outliers, and allow missing data and non-normal distribution of data (Gilbert, 1987; Salmi et al., 2002), appropriate for the analysed data set. The Mann–Kendall method is appropriate for detection of monotonic trends in data series that have no seasonal variation or autocorrelation. Atmospheric concentrations and deposition fluxes of N_r species, however, generally have distinct seasonal variability (Pan et al., 2012) and the Mann–Kendall test is thus applied to annual values.

Satellite observations during 2005–2015 indicate that tropospheric NO_2 levels peaked in 2011 over China (Krotkov et al., 2016; Duncan et al., 2016) and NO_x emissions peaked in 2011/2012 (Miyazaki et al., 2017; van der A et al., 2017; Souri et al., 2017). To assess the impact of emission control measures on measured N_r concentrations and deposition fluxes at different land use types, we compared arithmetic mean values averaged from the last 3-year pe-

riod (2013–2015) with those averaged from the first 2-year period (2011–2012) for monitoring sites with continuous 5-year measurements (21 sites for dry, and 17 sites for wet/bulk). Seasonal concentrations and deposition fluxes of measured N_r species were calculated using the arithmetic average of matched seasons during the sampling periods; spring refers to March–May, summer covers June–August, autumn refers to September–November, and winter covers December–February.

3 Results

3.1 Spatial variability in concentrations of N_r species in air and precipitation

Summary statistics of monthly mean concentrations of NH_3 , NO_2 , HNO_3 , pNH_4^+ , and pNO_3^- at the 27 monitoring sites during 2011–2015 are listed in Table S2 of the Supplement. Monthly mean concentrations of NH_3 , NO_2 , HNO_3 , pNH_4^+ , and pNO_3^- ranged over 0.16–39.57 (TJ and WJ), 0.55–29.06 (LS and WJ), 0.04–4.93 (YQ and CAU), 0.11–57.20 (ZY and QZ), and 0.01–32.06 $\mu g N m^{-3}$ (DL and ZZ) respectively. On the basis of geographical location and classification of each site, the annual mean concentrations of each N_r species were calculated for three land use types in eastern China and its northern and southern regions (Table 1).

In eastern China, annual mean concentrations of NH_3 , NO_2 , HNO_3 , pNH_4^+ , and pNO_3^- at the urban sites (averages for the 5-year, 1.6 ± 0.2 (for HNO_3) to 10.2 ± 1.0 (for NO_2) $\mu g N m^{-3}$) increased by 18, 70, 33, 23, and 43 % respectively compared with their corresponding concentrations at the rural sites (1.2 ± 1.0 (for HNO_3) to 7.2 ± 0.9 (for NH_3) $\mu g N m^{-3}$); they also increased by 78–118 % compared with the concentrations at the background sites (0.9 ± 0.1 (for HNO_3) to 5.2 ± 0.3 (for NO_2) $\mu g N m^{-3}$; Table 1). Analogous patterns also occurred for all measured N_r in each region, except for NH_3 and pNH_4^+ in the northern region, for which the mean concentrations were 18 and 7 % lower at the urban sites than at the rural sites respectively.

Comparing northern vs. southern regions (Table 1), at urban sites the annual mean concentrations of NH_3 , HNO_3 , and pNH_4^+ showed smaller non-significant differences ($-1 \sim 9$ %), whereas NO_2 and pNO_3^- showed larger non-significant increases (34 and 76 % respectively) in the north. By contrast, the mean concentrations of all measured N_r species were significantly ($p < 0.05$) higher (by 40–104 %) at rural sites in northern region. Similarly, individual concentrations at background sites were 21–71 % higher in the northern than southern region. Averaged across three land use types, the annual mean N_r concentrations of five N_r species in the north increased to varying extents (by 84 % for pNO_3^- , 63 % for pNH_4^+ , 57 % for NH_3 , 47 % for NO_2 , and 28 % for HNO_3) compared with those in the south. The annual concentrations of total N_r (i.e. the sum of five N_r

species) decreased in the order urban > rural > background in eastern China as a whole and in the north and south regions; further, the annual total N_r concentrations at urban and background sites were 17 and 34 % higher ($p > 0.05$) in the north than in the south respectively, whereas those at northern rural sites ($31.6 \pm 3.8 \mu g N m^{-3}$) were significantly ($p < 0.05$) higher than the means at southern rural sites ($17.0 \pm 1.7 \mu g N m^{-3}$).

The monthly VWM concentrations of NH_4^+ -N, NO_3^- -N, and TIN (the sum of NH_4^+ -N and NO_3^- -N) were in the ranges 0.01–26.77 (BY and YC), 0.06–28.92 (XS and WJ), and 0.09–50.29 $mg N L^{-1}$ (XS and YC) respectively (Table S3, Supplement). In eastern China and in each region, the annual VWM concentrations of NO_3^- -N and TIN showed a declining trend of urban > rural > background, whereas those of NH_4^+ -N followed the order rural \geq urban > background (Table 1). Comparing northern and southern regions, the annual concentrations of NH_4^+ -N, NO_3^- -N, and TIN were comparable at urban and background sites, and were significantly ($p < 0.05$) higher at northern rural sites.

3.2 Annual variability in concentrations of N_r species in air and precipitation

During the 2011–2015 period the annual mean concentrations of measured N_r species in air exhibited no significant trends at the 21 selected sites except for NH_3 at 4 sites (ZZ, DL, ZMD, YL), HNO_3 at 3 sites (DL, LSD, BY), pNH_4^+ at 1 site (XS), and total N_r at 3 sites (ZMD, YL, WJ; Fig. S1a–f, Supplement). Similarly, no significant trends were found for the annual VWM concentrations of NH_4^+ -N, NO_3^- -N, and TIN in precipitation at the 17 selected sites, with the exception of NO_3^- -N at 1 site (SZ; Fig. S2a–c, Supplement).

Figure 2 compares annual average concentrations of all measured N_r species between the periods 2013–2015 and 2011–2012 for three land use types. In eastern China the mean concentrations of NH_3 and pNH_4^+ showed non-significant increases (10–38 %) at all land use types except pNH_4^+ at background sites, which showed a small reduction (8 %; Fig. 2a, d). By contrast, the mean concentrations of remaining N_r species at three land use types showed smaller and non-significant changes: $-8 \sim 3$ % for NO_2 (Fig. 2b), $-13 \sim 5$ % for HNO_3 (Fig. 2c), and $-1 \sim 5$ % for pNO_3^- (Fig. 2e). The relative changes in the annual total N_r concentration were also not significant, with the largest increase at rural sites (16 %) and smaller increases at urban (4 %) and background (1 %) sites (Fig. 2f). Separated by regions, annual mean concentrations of five N_r species at three land use types mostly showed increases (4–57 %) in the north, and reductions (0.3–21 %) in the south (Fig. 2a–f). The relative changes in individual concentrations at northern rural sites (9 % reduction for HNO_3 , and 9–52 % increases for the other species) and southern rural sites (4 % increase for pNH_4^+ , and 0.3–21 % reductions for other species) were not significant. The annual total N_r concentrations showed small rela-

Table 1. Annual average (standard error) concentrations of various N_r compounds in air and precipitation at different land use types in eastern China and its northern and southern regions for the 5-year period 2011–2015.

Region ^a	LUT ^b	Ambient conc. $\mu\text{g N m}^{-3}$					Rainwater conc. mg NL^{-1}			
		NH_3	NO_2	HNO_3	$p\text{NH}_4^+$	$p\text{NO}_3^-$	Total N_r	NH_4^+	NO_3^-	TIN
EC	urban	8.5	10.2	1.6	8.2	4.0	32.6	1.6	1.9	3.5
	(<i>n</i> = 6)	(1.4)	(1.0)	(0.2)	(1.8)	(0.8)	(4.1)	(0.3)	(0.2)	(0.5)
	rural	7.2	6.0	1.2	6.7	2.8	23.9	1.7	1.4	3.1
	(<i>n</i> = 17)	(0.9)	(0.5)	(0.1)	(1.1)	(0.3)	(2.7)	(0.2)	(0.2)	(0.4)
BKD ^c		3.9	5.2	0.9	4.5	1.9	16.4	1.4	1.2	2.6
	(<i>n</i> = 4)	(0.6)	(0.3)	(0.1)	(0.4)	(0.3)	(1.4)	(0.3)	(0.4)	(0.6)
NREC	urban	8.1	11.7	1.6	8.6	5.1	35.1	2.2	2.4	4.6
	(<i>n</i> = 3)	(2.4)	(1.6)	(0.3)	(2.3)	(1.4)	(7.7)	(0.4)	(0.2)	(0.4)
	rural	9.9	7.4	1.4	9.2	3.7	31.6	2.4	2.0	4.4
	(<i>n</i> = 8)	(1.2)**	(0.7)*	(0.1)*	(1.9)*	(0.5)*	(3.8)**	(0.3)**	(0.2)**	(0.4)**
BKD		4.7	5.7	1.0	5.1	2.4	18.8	1.8	1.5	3.3
	(<i>n</i> = 2)	(0.6)	(0.3)	(0.1)	(0.2)	(0.3)	(0.1)	(0.2)	(0.3)	(0.1)
SREC	urban	8.9	8.7	1.6	7.9	2.9	30.1	1.1	1.5	2.6
	(<i>n</i> = 3)	(1.8)	(0.6)	(0.1)	(3.1)	(0.2)	(4.5)	(0.3)	(0.3)	(0.6)
	rural	4.9	4.6	1.0	4.5	1.9	17.0	1.1	0.9	2.0
	(<i>n</i> = 9)	(0.6)	(0.6)	(0.1)	(0.6)	(0.2)	(1.7)	(0.2)	(0.1)	(0.3)
BKD		3.1	4.7	0.8	4.0	1.4	14.0	1.0	0.6	1.6
	(<i>n</i> = 2)	(0.7)	(0.4)	(0.1)	(0.2)	(0.2)	(0.6)	(0.0)	(0.0)	(0.0)

^a EC: eastern China; NREC: northern region of eastern China; SREC: southern region of eastern China. ^b LUT: land use type; *n* denotes number of monitoring sites. ^c BKD: Background. "conc": concentration. * and ** denote significance at the 0.05 and 0.01 probability levels for difference in annual mean N_r concentrations at a given site type between northern and southern regions respectively.

tive changes (from -1 to 5%) across all land use types in the two regions, except at northern rural sites, which exhibited a larger but non-significant increase (25% ; Fig. 2f). Due to significant interannual variability, longer records are needed to better assess the significance of any concentration changes.

In eastern China, the annual VWM concentrations of $\text{NH}_4^+\text{-N}$, $\text{NO}_3^-\text{-N}$, and TIN showed the largest increase of $26\text{--}31\%$ at background sites, a smaller increase of $4\text{--}5\%$ at rural sites, and a decrease of $2\text{--}14\%$ at urban sites; however, those changes were not significant (Fig. 2g–i). Regionally, their respective concentrations showed increases ($3\text{--}45\%$) in the north and reductions ($5\text{--}33\%$) in the south, except for a small increase (4%) in $\text{NH}_4^+\text{-N}$ at background sites.

3.3 Seasonal variability in concentrations of N_r species in air and precipitation

Figure 3 shows seasonal patterns of NH_3 , NO_2 , HNO_3 , $p\text{NH}_4^+$, $p\text{NO}_3^-$, and total N_r concentrations for three land use types in eastern China and its northern and southern regions, averaged from corresponding measurements at the 27 study sites (details for each site are given in Tables S4–S9 of the Supplement). Average NH_3 concentrations at all land use types decreased in the order summer > spring > autumn > winter, and significant seasonal differences generally occurred between summer and winter (Fig. 3a). Conversely, the average NO_2 concentration gen-

erally showed the highest value in winter and the lowest in summer; differences between seasonal concentrations were sometimes significant at rural sites in the south and background sites, but not at urban sites (Fig. 3b). The seasonal changes in the HNO_3 concentration were generally small and not significant for all land use types (Fig. 3c).

The average $p\text{NH}_4^+$ concentration exhibited a non-significant seasonal variation across all land use types, except for southern rural sites which showed significantly higher values in winter than in summer (Fig. 3d). The highest $p\text{NH}_4^+$ concentrations mostly occurred in winter. The average $p\text{NO}_3^-$ concentrations at all land use types followed the order winter > spring \approx autumn > summer; the seasonal changes are sometimes significant, except for urban sites in eastern China and its northern region (Fig. 3e). The average concentration of total N_r usually showed small and non-significant seasonal differences for all land use types (Fig. 3f).

In eastern China and its two regions, the seasonal VWM concentrations of $\text{NH}_4^+\text{-N}$, $\text{NO}_3^-\text{-N}$, and TIN in precipitation at three land use types (averaged from the 27 sites, details in Tables S10–S12 of the Supplement) showed a similar seasonal pattern, with the highest values in winter and the lowest in summer or autumn (Fig. 4a–c). Significant seasonal differences usually occurred between winter and the other three

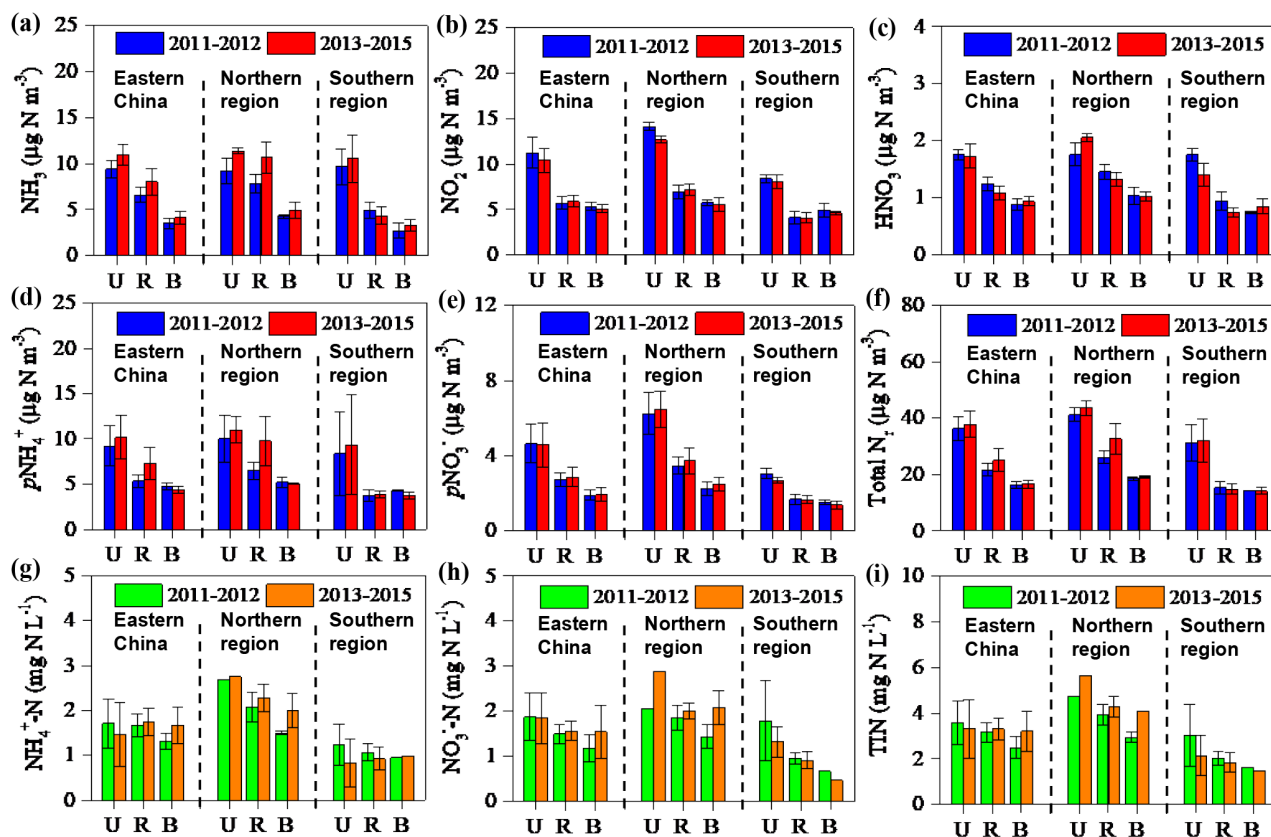


Figure 2. Comparison of annual mean concentrations of (a) NH_3 , (b) NO_2 , (c) HNO_3 , (d) $p\text{NH}_4^+$, and (e) $p\text{NO}_3^-$; (f) total N_r , i.e. the sum of all measured N_r in air; volume-weighted concentrations of NH_4^+ (g); NO_3^- (h); total inorganic N (TIN): sum of NH_4^+ and NO_3^- (i), in precipitation between the 2011–2012 period and the 2013–2015 period for different land use types in eastern China and its northern and southern regions. U, R, and B denote urban, rural, and background sites respectively. The number of sites for each land use type in each region can be found in Table S1 in the Supplement. The error bars are the standard errors of means.

seasons at all land use types, except background sites and southern urban sites.

3.4 Spatial variability in dry and wet/bulk N deposition of N_r species

Dry deposition fluxes of NH_3 , HNO_3 , NO_2 , $p\text{NH}_4^+$, and $p\text{NO}_3^-$ ranked in the order urban > rural > background in eastern China and in both southern and northern regions (except for $p\text{NH}_4^+$ in the north; Table 2). Comparing northern and southern regions, at urban sites the mean dry $p\text{NH}_4^+$ deposition was slightly higher (2 %) in the north, whereas larger enhancements (24–69 %) in the mean fluxes were found in the north for the remaining N_r species. By contrast, individual fluxes were significantly higher (by 64–138 %) at northern rural sites, except for HNO_3 , which showed a large non-significant increase (58 %). At northern background sites, the mean dry deposition fluxes of NH_3 and NO_2 were much higher (159 %) and lower (68 %) respectively; however, only small differences in the means were found for HNO_3 (6 % lower in the north), $p\text{NH}_4^+$ (5 % lower), and $p\text{NO}_3^-$ (14 %

higher). The spatial pattern of total N dry deposition flux (the sum of the fluxes of the five N_r species) by land use types ranked in the same order as individual N_r species in eastern China. Compared with the southern region, mean total N fluxes in the north region were significantly higher (by 85 %) at rural sites, but showed non-significant increases at urban and background sites (33 and 38 % respectively).

The wet/bulk deposition fluxes of $\text{NH}_4^+\text{-N}$, $\text{NO}_3^-\text{-N}$, and TIN ranked in the order urban > rural > background in eastern China and in each region (except for $\text{NH}_4^+\text{-N}$ in the south; Table 2). In addition, their respective fluxes were generally comparable in northern and southern regions.

3.5 Annual variability in dry and wet/bulk N deposition

The annual trends of dry deposition fluxes of individual N_r species at the 21 selected sites are consistent with trends in their respective ambient concentrations, except for HNO_3 at three sites (SZ, LSD, and ZY; Figs. S3a–e and S1a–e, Supplement). A consistent picture is also seen for the total

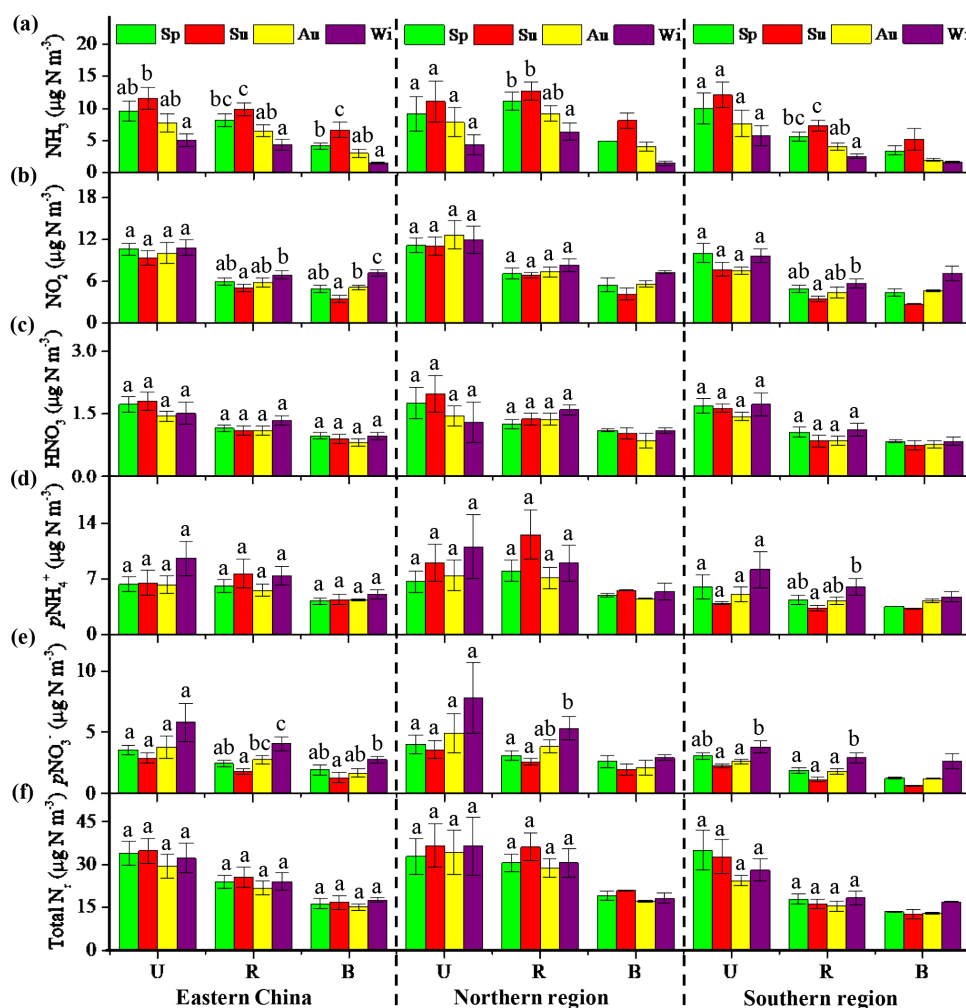


Figure 3. Seasonal mean concentrations averaged over 2011–2015 of (a) NH_3 , (b) NO_2 , (c) HNO_3 , (d) $p\text{NH}_4^+$, (e) $p\text{NO}_3^-$, and (f) total N_r , i.e. the sum of all measured N_r in air, at different land use types in eastern China and its northern and southern regions. Sp, Su, Au, and Wi represent spring, summer, autumn, and winter respectively. U, R, and B denote urban, rural, and background sites respectively. The number of sites for each land use type in each region can be found in Table 1. The error bars are the standard errors of means, and values without same letters on the bars denote significant differences between the seasons ($p < 0.05$).

dry N deposition fluxes at all but two sites (DL and WJ; Figs. S3f and S1f, Supplement). Similarly, the annual trends of wet/bulk deposition fluxes of NH_4^+ -N, NO_3^- -N, and TIN at 17 selected sites are similar to their respective concentrations in precipitation (Fig. S4a–c, Supplement).

In eastern China the annual average dry deposition fluxes of NH_3 , NO_2 , HNO_3 , $p\text{NH}_4^+$, and $p\text{NO}_3^-$ showed non-significant increases (2–39%) or reductions (1–19%) between the periods 2011–2012 and 2013–2015 at the three land use types (Fig. 5a–e), similar in sign and magnitude to their respective concentrations described earlier. The annual average total N dry deposition fluxes showed small and non-significant increases across the study periods: 2% at urban sites, 9% at rural sites, and 7% at background sites (Fig. 5f). The sign and magnitude of period-to-period changes in dry

deposition and ambient concentrations of all measured N_r species were generally similar between the southern and northern regions.

Wet/bulk deposition fluxes of NH_4^+ -N, NO_3^- -N, and TIN generally decreased (4–29%) between 2011–2012 and 2013–2015 at all land use types in eastern China; one exception was NO_3^- -N, which exhibited a small increase (3%) at urban sites (Fig. 5g–i). Similar tendencies were also observed in both northern and southern regions.

3.6 Seasonal variability in dry and wet/bulk deposition of N_r species

Seasonal variations of dry deposition of individual N_r species at each site are shown in Tables S4–S9 in the Supple-

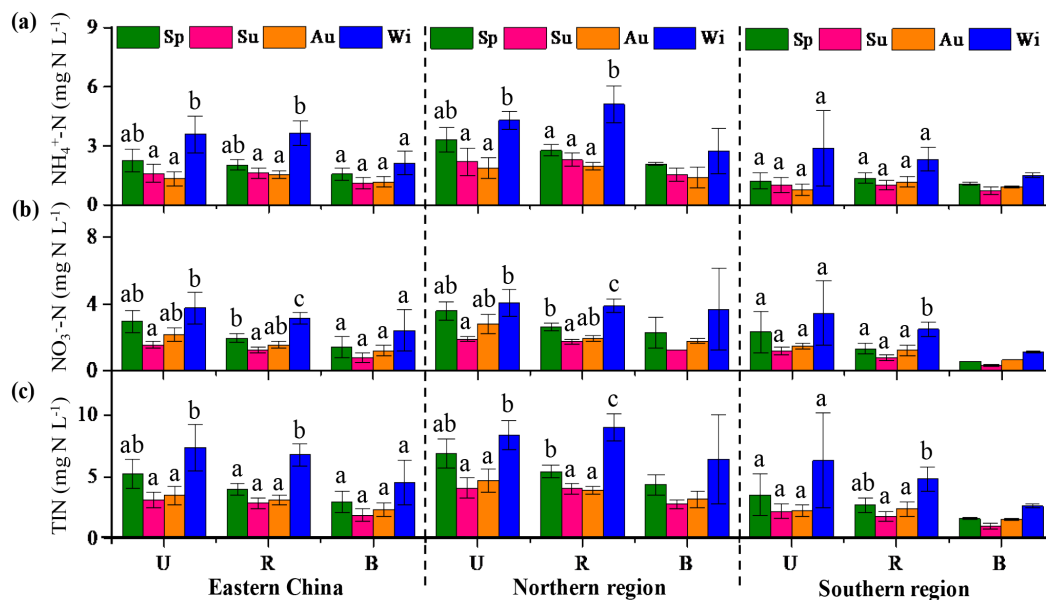


Figure 4. Seasonal mean concentrations averaged over 2011–2015 of NH_4^+ (a), NO_3^- (b), and total inorganic N (TIN), i.e. the sum of NH_4^+ and NO_3^- (c), in precipitation at different land use types in eastern China and its northern and southern regions. Sp, Su, Au, and Wi represent spring, summer, autumn, and winter respectively. U, R, and B denote urban, rural, and background sites respectively. The number of sites for each land use type in each region can be found in Table 1. The error bars are the standard errors of means, and values without same letters on the bars denote significant differences between the seasons ($p < 0.05$).

Table 2. Annual average (standard error) dry and wet/bulk deposition fluxes ($\text{kg N ha}^{-1} \text{ yr}^{-1}$) of various N_r compounds at different land use types in eastern China and its northern and southern regions for the 5-year period 2011–2015.

Region ^a	LUT ^b	Dry deposition					Wet/bulk deposition			
		NH_3	NO_2	HNO_3	$p\text{NH}_4^+$	$p\text{NO}_3^-$	Total N_r	NH_4^+	NO_3^-	TIN
EC	Urban	12.6	4.4	7.7	4.8	2.1	31.7	12.6	15.4	28.0
	($n = 6$)	(1.4)	(1.2)	(1.6)	(1.4)	(0.5)	(4.6)	(1.9)	(0.7)	(2.2)
	Rural	9.1	2.9	4.6	4.0	1.5	22.1	11.9	10.2	22.1
	($n = 17$)	(0.9)	(0.3)	(0.6)	(0.7)	(0.2)	(2.3)	(1.0)	(0.5)	(1.4)
BKD ^c		7.9	1.8	3.5	1.9	0.8	15.8	10.7	7.7	18.4
	($n = 4$)	(2.1)	(0.6)	(0.2)	(0.3)	(0.1)	(1.5)	(1.8)	(0.3)	(1.8)
NREC	Urban	13.9	5.2	9.4	4.9	2.7	36.2	13.9	14.1	28.0
	($n = 3$)	(1.9)	(2.5)	(3.0)	(1.9)	(1.0)	(8.2)	(3.5)	(1.0)	(4.4)
	Rural	12.1**	3.6*	5.7	5.7*	2.1**	29.3**	12.3	10.3	22.6
	($n = 8$)	(1.3)	(0.4)	(1.0)	(1.2)	(0.3)	(3.2)	(1.3)	(0.7)	(1.8)
BKD		11.4	0.9	3.4	1.9	0.8	18.4	7.8	7.6	15.4
	($n = 2$)	(0.6)	(0.7)	(0.3)	(0.7)	(0.2)	(0.7)	(1.4)	(0.8)	(0.6)
SREC	Urban	11.2	3.6	5.9	4.8	1.6	27.2	11.4	16.6	28.0
	($n = 3$)	(2.0)	(0.3)	(0.6)	(2.6)	(0.2)	(4.0)	(2.0)	(0.4)	(2.1)
	Rural	6.5	2.2	3.6	2.4	1.0	15.8	11.6	10.2	21.8
	($n = 9$)	(0.5)	(0.4)	(0.6)	(0.4)	(0.2)	(1.4)	(1.5)	(0.9)	(2.2)
BKD		4.4	2.7	3.6	2.0	0.7	13.3	13.6	7.9	21.5
	($n = 2$)	(1.0)	(0.2)	(0.3)	(0.1)	(0.1)	(0.7)	(0.1)	(0.1)	(0.1)

^a EC: eastern China; NREC: northern region of eastern China; SREC: southern region of eastern China. ^b LUT: land use type; n denotes number of monitoring sites. ^c BKD: Background. * and ** denote significance at the 0.05 and 0.01 probability levels for difference in annual mean N_r concentrations at a given site type between northern and southern regions respectively.

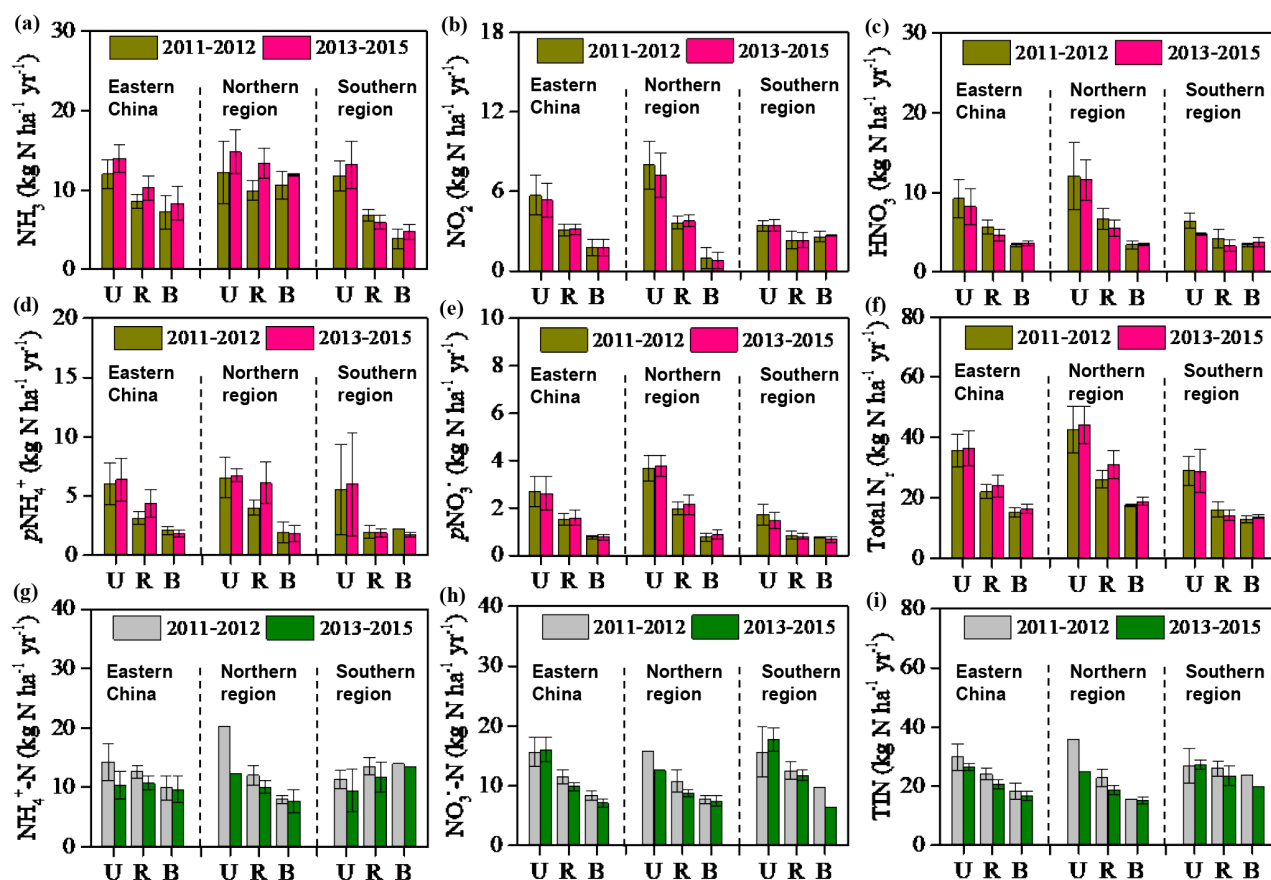


Figure 5. Comparison of dry deposition of (a) NH_3 , (b) NO_2 , (c) HNO_3 , (d) $p\text{NH}_4^+$, (e) $p\text{NO}_3^-$, and (f) total N_r : sum of all measured N_r in air and wet/bulk deposition of NH_4^+ (g); NO_3^- (h), and total inorganic N (TIN): sum of NH_4^+ and NO_3^- (i), in precipitation between the 2011–2012 period and the 2013–2015 period for different land use types in eastern China and its northern and southern regions. U, R, and B denote urban, rural, and background sites respectively. The number of sites for each land use type in each region can be found in Table S1 in the Supplement. The error bars are the standard errors of means.

ment. In eastern China and in each region, dry NH_3 deposition fluxes at all land use types followed the order summer > spring > autumn > winter, with the seasonal changes usually significantly different (Fig. 6a). Similarly, the dry NO_2 deposition flux was also at its minimum in winter, but its maximum was found in summer at urban and rural sites and in autumn at background site; seasonal differences in most cases were not significant (Fig. 6b). Seasonal patterns of dry HNO_3 deposition flux at all land use types were similar to those for dry NH_3 deposition fluxes, and the resulting seasonal changes were sometimes significant, except at northern urban sites (Fig. 6c).

Dry $p\text{NH}_4^+$ deposition fluxes peaked in spring or summer at urban and rural sites, but remained at similar levels across the four seasons at background sites; however, no significant seasonal variations were found at any land use types except for rural sites in the north (Fig. 6d). Dry $p\text{NO}_3^-$ deposition fluxes were higher in spring and winter than in summer and autumn at all land use types, and the seasonal changes were

sometimes significant at background sites and at southern urban and rural sites (Fig. 6e). Total dry N deposition fluxes at all land use types showed similar seasonal variations to dry NH_3 deposition, with the highest values in summer and the lowest in winter; significant seasonal differences generally were observed between winter and the other three seasons (Fig. 6f).

Wet/bulk deposition fluxes of NH_4^+ -N, NO_3^- -N, and TIN all showed significant seasonal variation at urban and rural sites, but not at background sites, with the highest values in summer and the lowest in winter (Fig. 7a–c).

3.7 Spatial–temporal variability in total annual dry and wet/bulk deposition of N_r species

In eastern China total annual mean N deposition (dry plus wet/bulk) fluxes at rural and background sites were comparable (on average 44.3 ± 3.0 and $34.3 \pm 0.7 \text{ kg N ha}^{-1} \text{ yr}^{-1}$ respectively), but significantly lower than those at urban sites ($59.7 \pm 6.1 \text{ kg N ha}^{-1} \text{ yr}^{-1}$; Table 2, and Fig. S5, Supple-

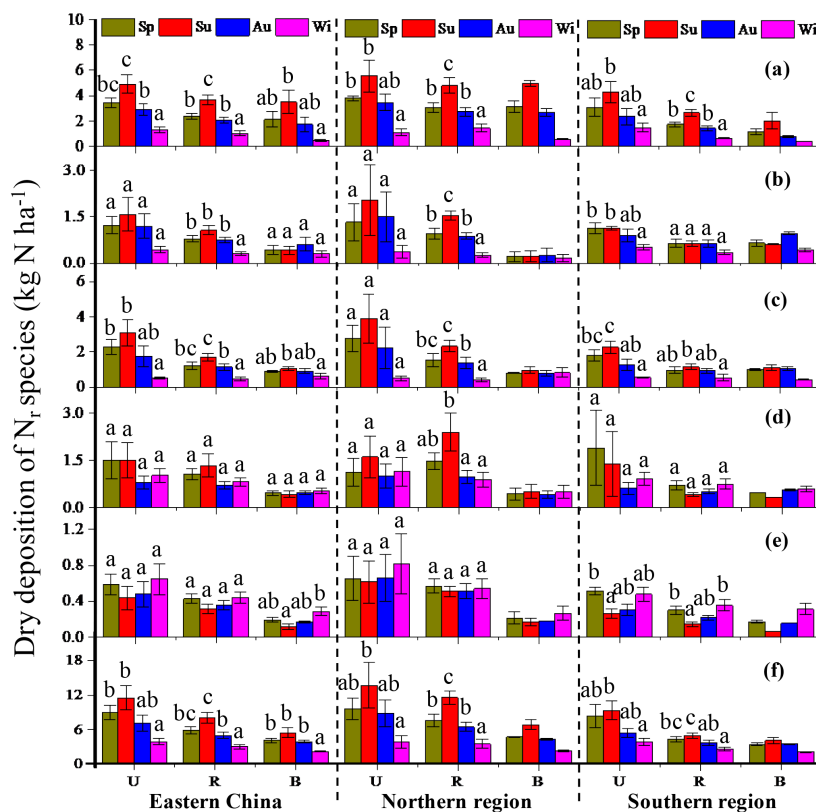


Figure 6. Seasonal mean dry deposition averaged over 2011–2015 of (a) NH₃, (b) NO₂, (c) HNO₃, (d) pNH₄⁺, (e) pNO₃⁻, and (f) total N_r, i.e. the sum of all measured N_r, in air at different land use types in eastern China and its northern and southern regions. Sp, Su, Au, and Wi represent spring, summer, autumn, and winter respectively. U, R, and B denote urban, rural, and background sites respectively. The number of sites for each land use type in each region can be found in Table 2. The error bars are the standard errors of means, and values without same letters on the bars denote significant differences between the seasons ($p < 0.05$).

ment). Similar tendencies for total N deposition fluxes were observed in the southern region, while in the north a significant difference was only found between urban and background sites (Fig. S5, Supplement). From 2011 to 2015, no significant annual trend was found in the total N deposition at 16 selected sites (Fig. S6a, Supplement). The total annual mean N deposition fluxes at three land use types showed small and non-significant reductions (1–5 %) between 2011–2012 and 2013–2015 (Fig. S6b, Supplement). Regionally, the total fluxes at each land use type were of similar magnitude in the two periods. Also, the ratio of NH_x (wet/bulk NH₄⁺-N deposition plus dry deposition of NH₃ and particulate NH₄⁺) to NO_y (wet/bulk NO₃⁻-N deposition plus dry deposition of NO₂, HNO₃ and particulate NO₃⁻) showed a non-significant annual trend across all sites (Fig. 8a). At all land use types, the averaged ratios were slightly higher in the 2013–2015 period than in the 2011–2012 period (Fig. 8b).

4 Discussion

4.1 Comparisons of NH₃ and NO₂ measurements with satellite data

Eastern China is a highly industrialized and polluted region, and has been proven to be a hotspot of N_r (NH₃ and NO_x) emissions and deposition globally (Vet et al., 2014; Kanakidou et al., 2016). The results presented above showed that, in eastern China, annual mean concentrations of measured N_r species in air and precipitation were generally higher in the north than in the south (Table 1). This is likely due to higher consumption of energy and application of N fertilizers, along with lower precipitation amounts in the north, previously identified as key factors affecting spatial patterns of N deposition in China (Liu et al., 2013; Jia et al., 2014; Zhu et al., 2015). Because only 27 sites covering a range of land use types were included in the present study, additional information would be valuable in determining whether the observed spatial patterns adequately represent conditions in eastern China. To address this issue, we use measured NH₃

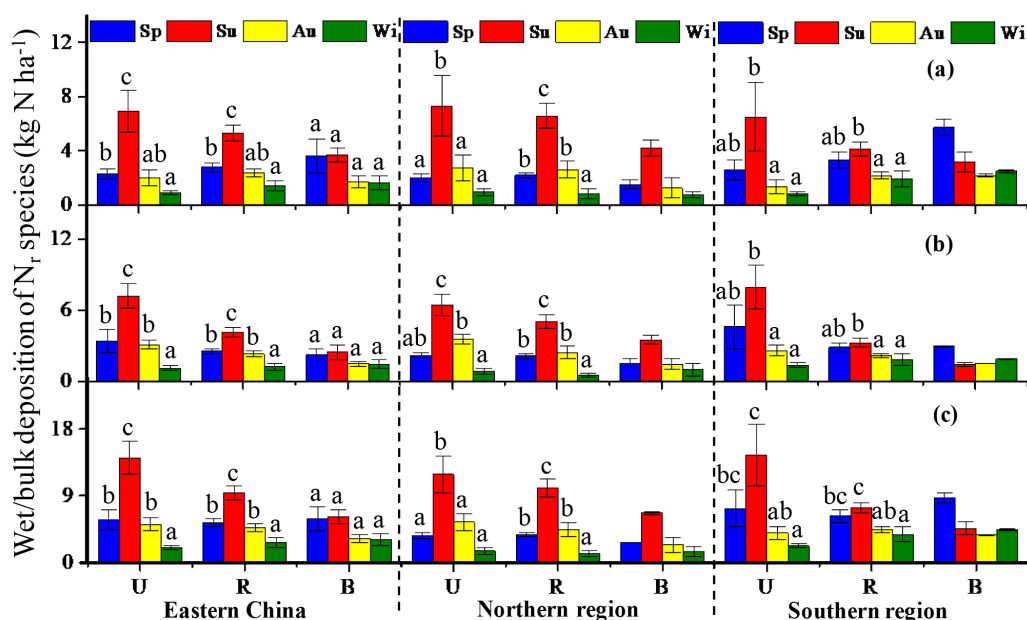


Figure 7. Seasonal mean wet/bulk deposition averaged over 2011–2015 of NH_4^+ (a), NO_3^- (b), and total inorganic N (TIN), i.e. the sum of NH_4^+ and NO_3^- (c), in precipitation at different land use types in eastern China and its northern and southern regions. Sp, Su, Au, and Wi represent spring, summer, autumn, and winter respectively. U, R, and B denote urban, rural, and background sites respectively. The number of sites for each land use type in each region can be found in Table 2. The error bars are the standard errors of means, and values without same letters on the bars denote significant differences between the seasons ($p < 0.05$).

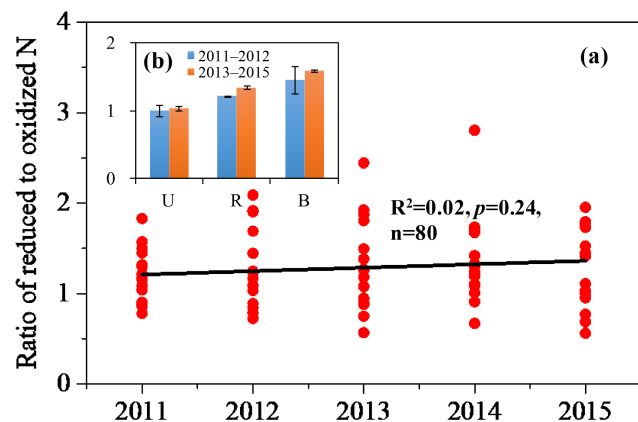


Figure 8. Annual trend of the ratio of NH_x (wet/bulk NH_4^+ -N deposition plus dry deposition of NH_3 and particulate NH_4^+) to NO_y (wet/bulk NO_3^- -N deposition plus dry deposition of NO_2 , HNO_3 and particulate NO_3^-) across 16 selected sites (a), with a comparison between the 2011–2012 period and the 2013–2015 period for different land use types in eastern China (b). U, R, and B denote urban, rural, and background sites respectively. The number of sites with the same land use type can be found in Fig. S6 in the Supplement.

and NO_2 concentrations to evaluate remote sensing techniques for retrieving NH_3 and NO_2 concentrations. If accurate, these remote sensing techniques are well suited to ascer-

tain regional species distributions. NH_3 and NO_x are primary emissions with important anthropogenic emissions (Fowler et al., 2013). NO , the main component of emitted NO_x , is oxidized in the atmosphere to NO_2 . NO_2 is further oxidized via daytime or nighttime chemistry to HNO_3 (Khoder, 2002). NH_3 and HNO_3 can react to form fine particle ammonium nitrate (Seinfeld and Pandis, 2006). Thus, spatial patterns of NH_3 and NO_2 observed from space can be useful indicators of reduced and oxidized N_r pollution over eastern China.

From satellite observations (Fig. 9a, b), it can be seen that both IASI_ NH_3 and OMI_ NO_2 columns show clearly higher values over the northern region of eastern China. Overall, satellite observations and surface measurements for NH_3 and NO_2 (plotted on the maps of Fig. 9a, b) show a similar spatial pattern. Significant positive correlations were found between IASI_ NH_3 column observations and NNDMN_ NH_3 measurements ($r = 0.72$, $p < 0.001$; Fig. 9c) and between OMI_ NO_2 observations and NNDMN_ NO_2 measurements ($r = 0.86$, $p < 0.001$; Fig. 9d) at the 27 surface measurement locations, suggesting that satellite measurements of NH_3 and NO_2 can be used to capture regional differences in NH_3 and NO_2 pollution. Looking beyond the surface measurement location, the satellite observations further confirm the existence of greater N_r pollution in the northern region of eastern China than in the southern region.

To further explore temporal concentration variability, monthly mean satellite NH_3 and NO_2 columns are compared

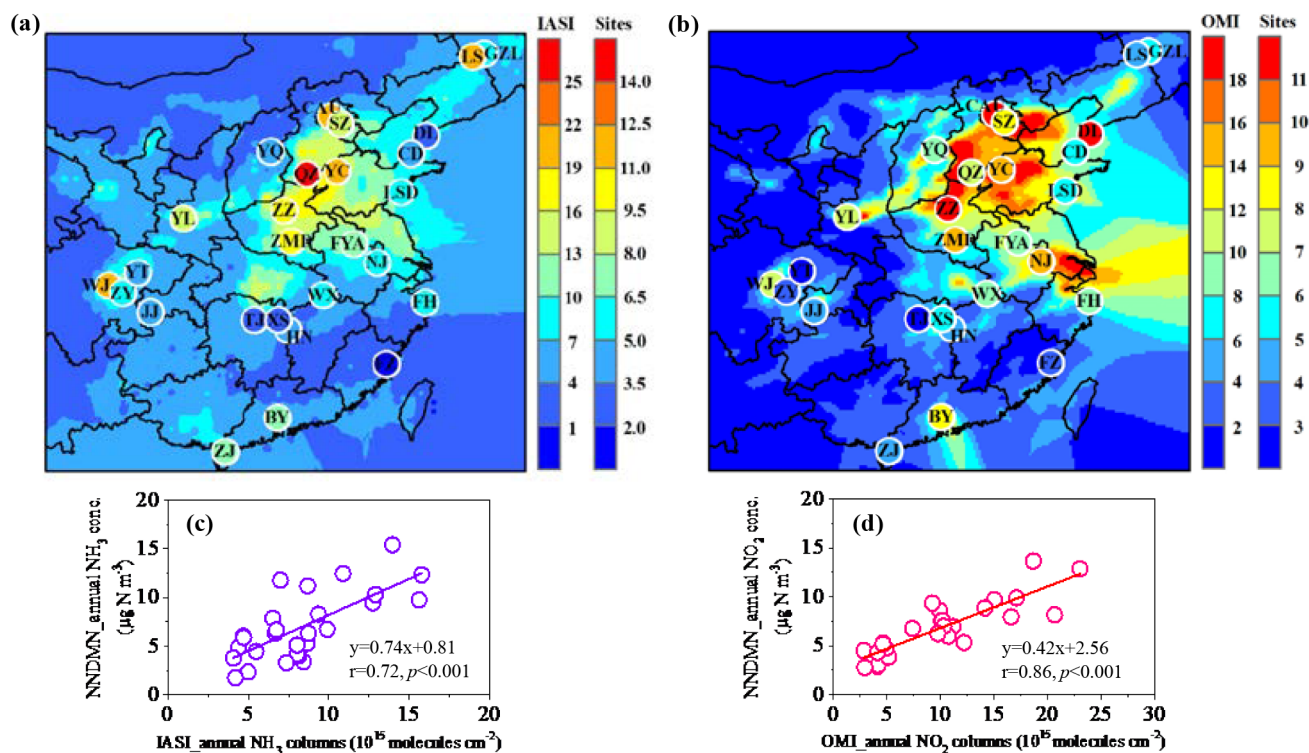


Figure 9. Spatial variation of atmospheric N_r in eastern China: (a) NNDMN_NH₃ concentrations vs. IASI_NH₃ columns; (b) NNDMN_NO₂ concentrations vs. OMI_NO₂ columns; (c) relationship of NNDMN_NH₃ concentrations vs. IASI_NH₃ columns; (d) relationship of NNDMN_NO₂ concentrations vs. OMI_NO₂ columns.

with monthly mean ground concentrations of NH₃ and NO₂ (Figs. S7 and S8, Supplement). The linear correlation between satellite columns and surface NH₃ concentrations is significant ($p < 0.05$) at the 10 sites ($r = 0.32$ – 0.87) in the northern region and at 4 sites ($r = 0.46$ – 0.84) in the southern region (Fig. S7, Supplement), while the linear correlation between satellite columns and surface NO₂ concentrations is significant at the 10 sites ($r = 0.28$ – 0.68) in the northern region and 9 sites ($r = 0.36$ – 0.66) in the southern region (Fig. S8, Supplement). These results indicate that the OMI_NO₂ retrieval can well capture the temporal variations of surface NO₂ concentrations over eastern China, whereas the IASI_NH₃ retrievals better capture temporal variability in surface concentrations for the northern region. The weak correlations observed between IASI_NH₃ observations and surface measurements at 10 of the 14 sites in the southern region (Fig. S7, Supplement) suggest that the IASI_NH₃ observations need to be improved for investigating temporal variability in NH₃ concentration, despite the satellite observation being at a specific time of day, that is, while the surface concentrations integrate across the diurnal cycle of emissions and mixing layer evolution. It should be noted that a direct comparison between surface concentration and satellite column measurements is inevitably affected by many factors, such as changes in boundary layer height, vertical profiles

of species, and interferences from cloud and aerosol (Van Damme et al., 2015). Nevertheless, the ratio of satellite column to surface concentration measurements is meaningful as it can provide insight into sensitivity of a satellite retrieval to variation in the concentration of a gas in the surface layer (Meng et al., 2008). To make a more accurate comparison, the vertical profile is recommended to convert the columns to the ground concentrations in future work.

4.2 Seasonal variations of N_r concentration and deposition

The seasonal concentrations of N_r species in air and precipitation are dependent on their sources and meteorological conditions. The highest concentrations of NH₃ in summer at all land use types (Fig. 3a) are most likely due to enhanced NH₃ emissions from natural and fertilized soils, and biological sources such as humans, sewage systems, and organic waste in garbage containers (Chang et al., 2016; Meng et al., 2018). Zhang et al. (2018) showed that NH₃ emissions in China show a strong summer peak, with emissions about 50 % higher in summer than spring and autumn. The lowest concentrations of NH₃, in winter (Fig. 3a), can be ascribed to low NH₃ volatilization under cold conditions, high snow coverage, and less agricultural activity (Cao et al., 2009) with large consumption of NH₃ to form NH₄NO₃

and $(\text{NH}_4)_2\text{SO}_4$. The lower NO_2 concentration in summer (Fig. 3b) might result from higher atmospheric mixing in a deeper boundary layer and a higher rate of oxidation of NO_2 to HNO_3 by reaction with OH (Atkins and Lee, 1995), which is more abundant in summer due to greater photochemical activity. Increased NO_2 emissions from greater coal combustion for domestic heating (from middle November to middle March) in northern China may also enhance NO_x emissions and subsequent NO_2 concentrations in autumn/winter (Zhao et al., 2011).

Particulate NH_4^+ and NO_3^- are mainly generated via chemical reactions between NH_3 and inorganic acids (e.g. HNO_3 , H_2SO_4). We found that concentrations of $p\text{NH}_4^+$ and $p\text{NO}_3^-$ at all land use types usually peaked in winter because low temperature and high emissions of NO_x and SO_2 are favourable for formation of NH_4NO_3 and $(\text{NH}_4)_2\text{SO}_4$ aerosols (Xu et al., 2016), consistent with higher concentrations of $p\text{NH}_4^+$ and $p\text{NO}_3^-$. In addition, in winter temperature inversions in combination with stable meteorological conditions (e.g. low wind speed) limit horizontal and vertical exchange of pollutants, and further elevated atmospheric $p\text{NH}_4^+$ and $p\text{NO}_3^-$ levels (F. Liu et al., 2017). In order to identify potential transport of NO_2 , $p\text{NH}_4^+$, and $p\text{NO}_3^-$ from northern region, we calculated 3-day backward trajectories arriving at five southern sites (Nanjing, Baiyun, Taojing, Ziyang, and Huinong) during January, April, July, and October using the TrajStat. The TrajStat analysis generally showed that the high proportions (overall 10–36 %) of air masses from the north to the south of eastern China occurred in the autumn/winter, suggesting that the transport of NO_2 , $p\text{NH}_4^+$, and $p\text{NO}_3^-$ from northern China would result in increases in their respective concentrations in autumn/winter south of the Qinling Mountains–Huaihe River line, except at Ziyang site (Fig. S9, Supplement).

Nitric acid is a secondary pollutant, formed through gas-phase reaction of NO_2 with the OH radical, reaction of NO_3 with aldehydes or hydrocarbons, or hydrolysis of N_2O_5 (Khoder, 2002). Nitric acid concentrations are expected to be further influenced by air temperature, relative humidity, and ambient NH_3 concentrations (Allen et al., 1989); fine particle NH_4NO_3 formation is favoured at low temperatures and high relative humidities. Due to a lack of information regarding primary formation pathways and influencing factors at our study sites, we cannot offer a definitive explanation for small and differing seasonal patterns of HNO_3 concentrations observed at the three land use types (Fig. 3c).

Ammonium-N and nitrate-N in precipitation mainly originate from corresponding reduced (e.g. NH_3 , $p\text{NH}_4^+$) and oxidized (e.g. HNO_3 , NO_2 , $p\text{NO}_3^-$) N in air, scavenged respectively by rain and/or snow events (Seinfeld and Pandis, 2006). At all land use types, the seasonal variation of NH_4^+ -N concentration in precipitation was opposite that of reduced N concentrations (the sum of NH_3 and $p\text{NH}_4^+$; Figs. 4a and S10a in the Supplement), whereas a similar seasonal pattern was found between NO_3^- -N and oxidized N (the sum of

HNO_3 , NO_2 , and $p\text{NO}_3^-$) concentrations (Figs. 4b and S10b in the Supplement). Higher precipitation amounts in summer could account for lower NH_4^+ -N concentrations in summer (Figs. 4a and S11 in the Supplement) due to a dilution effect (Xu et al., 2015). In contrast, seasonal variations of rainwater NO_3^- -N concentrations were more likely dominated by seasonal changes in oxidized N concentrations rather than precipitation amount.

The seasonal variation of NH_3 dry deposition is generally similar to that of NH_3 concentration (Figs. 3a and 6a). Given comparable seasonal mean V_d for NH_3 across the four seasons in most cases (Fig. S12a–c, Supplement), the seasonality of NH_3 deposition is mainly dominated by changes in ambient NH_3 concentrations. Seasonal deposition fluxes of NO_2 and HNO_3 both differ appreciably (Fig. 6b, c), showing similar variation to seasonality of their respective V_d values (Fig. S12d–i, Supplement). Given weaker seasonal fluctuations of NO_2 and HNO_3 concentrations, the seasonality of NO_2 and HNO_3 dry deposition are primarily functions of changes in V_d . Similar analyses suggest that seasonal variation of $p\text{NO}_3^-$ dry deposition was mainly caused by differences in seasonal $p\text{NO}_3^-$ concentrations (Figs. 3e and 6e), whereas that of $p\text{NH}_4^+$ dry deposition was primarily driven by seasonal changes in V_d (Figs. 6c and S12j–l, Supplement).

4.3 The role of NH_3 in mitigation of N_r air pollution

The latest pollutant emissions statistics from the Chinese Ministry of Environmental Protection (http://www.zhb.gov.cn/gkml/hbb/qt/201507/t20150722_307020.htm) showed that total annual emissions of SO_2 and NO_x were respectively reduced by 12.9 and 8.6 % in 2014 (approximately 9.9 and 6.3 Tg S yr^{-1} respectively), compared with those in 2010 (approximately 11.3 and 6.9 Tg S yr^{-1} respectively). This suggests that the goal set for the 12th FYP period was fulfilled ahead of time. Our field measurements demonstrate that annual mean concentrations of each N_r species and total N_r did not show significant decreasing trends at most sites during the 2011–2015 period (Fig. S1a–f, Supplement). Furthermore, annual mean total N_r concentrations showed non-significant increases (1–16 %) at three land use types during the 2013–2015 period compared with 2011–2012 (Fig. 2f). These results together suggest that N_r pollution may be not effectively mitigated in eastern China during the 12th FYP, likely due to the absence of NH_3 regulations, despite enforcement of a “Zero Increase Action Plan” by the Ministry of Agriculture for national fertilizer use (Liu et al., 2016).

Ammonia is the primary alkaline gas in the atmosphere. It plays an important role in formation of $(\text{NH}_4)_2\text{SO}_4$ and NH_4NO_3 aerosols (Seinfeld and Pandis, 2006). These secondary inorganic aerosols account for 40–57 % of the $\text{PM}_{2.5}$ concentrations in eastern China (Yang et al., 2011; Huang et al., 2014). Based on monthly mean molar concentrations, there were significant positive linear correlations between

NH_3 and $p\text{NH}_4^+$, NO_2 and $p\text{NO}_3^-$, SO_2 and $p\text{SO}_4^{2-}$, $p\text{NH}_4^+$ and $p\text{NO}_3^-$, and $p\text{NH}_4^+$ and $p\text{SO}_4^{2-}$ at all land use land types except for a non-significant relationship of NH_3 with $p\text{NH}_4^+$ at background sites (Fig. 10a–e). These results suggest that the precursor gases are responsible for the formation of secondary inorganic ions (i.e. $p\text{NH}_4^+$, $p\text{NO}_3^-$, and $p\text{SO}_4^{2-}$) locally at urban and rural sites, while secondary inorganic ions at background sites likely originated from long-distance transport. The ratio of concentrations of NH_3 to NH_x (NH_3 plus $p\text{NH}_4^+$) at urban (0.53 ± 0.15) and rural (0.52 ± 0.16) sites exceeded values at background (0.43 ± 0.16) sites. According to Walker et al. (2004), a value greater than 0.5 indicates that NH_x is more likely to be from local sources as opposed to long-range transport.

It is known that NH_3 in the atmosphere is preferentially neutralized by H_2SO_4 to form $(\text{NH}_4)_2\text{SO}_4$ and/or NH_4HSO_4 , with any remainder available for potential reaction with HNO_3 to form NH_4NO_3 . At urban and rural sites, monthly mean $p\text{NH}_4^+$ concentrations significantly positively correlated with the sum of $p\text{SO}_4^{2-}$ and $p\text{NO}_3^-$ concentrations (Fig. 10f). However, the slopes of regression equations between them were both smaller than unity (0.35 and 0.46 at urban and rural sites respectively), indicating an incomplete neutralization of acidic species (HNO_3 and H_2SO_4) by NH_3 at urban and rural sites. In other words, NH_3 is a factor limiting the formation of secondary inorganic ions. A model simulation by Wang et al. (2011) found that, without NH_3 emission controls, NO_3^- in $\text{PM}_{2.5}$ will be enhanced by 10 % in 2030 compared with 2005 in China, despite improved NO_x emissions controls. As reported by Zhang et al. (2017), total NH_3 emissions in China increased from $12.1 \text{ Tg N yr}^{-1}$ in 2000 to $15.6 \text{ Tg N yr}^{-1}$ in 2015 at an annual rate of 1.9 %. In contrast, total emissions of NO_x and SO_2 have decreased or stabilized in recent years, and were estimated to be 8.4 and $12.5 \text{ Tg S yr}^{-1}$ in 2014 respectively (Xia et al., 2016). Based on these factors, implementation of NH_3 control strategies, together with more stringent NO_x and SO_2 emission controls, should be considered to mitigate atmospheric N_r pollution.

4.4 The role of NH_3 emissions in control of N deposition

The present results showed that total dry N deposition fluxes at three land use types were higher in the northern region of eastern China than in the southern region (Table 1), mainly due to higher NH_3 dry deposition resulting from higher NH_3 concentrations in the north. This is especially true for northern rural sites (Table 1), mostly located in the North China Plain (NCP; see details in Xu et al., 2015). The NCP (that is, the plain areas in Beijing, Tianjin, Hebei, Henan, and Shandong provinces), a highly populated region with intensive agricultural production, contributes 30–40 % of the total annual NH_3 emissions in China (Huang et al., 2012). In addition, higher NH_3 concentration is also likely due to the

higher NH_3 volatilization in calcareous soils than that in the acidic red soil, as mentioned in Sect. 2.1. Total annual NH_3 emissions in northern region increased from 4.3 Tg N yr^{-1} in 2011 to 4.7 Tg N yr^{-1} in 2015 at an annual rate of 1.8 %. In contrast, the emissions of NO_x and SO_2 averaged 2.8 and 3.7 Tg S yr^{-1} during 2011–2015, and decreased at annual rates of 6.8 and 5.7 % respectively (details of the emissions will be illustrated in Sect. 4.5). Such reductions may enhance free NH_3 in the atmosphere. However, according to a modelling study by Han et al. (2017), the influence of removing anthropogenic SO_2 emissions on dry N deposition fluxes during 2010–2014 was quite weak, with the change within ~ -0.5 to $\sim 0.5 \text{ (kg N ha}^{-1} \text{ yr}^{-1})$ over most regions in China. Thus, we anticipate that reducing NH_3 emissions can effectively control N deposition.

To further examine contributions of NH_3 emissions to total (wet plus dry) N deposition at each site and over eastern China, we conducted model sensitivity tests using the nested GEOS-Chem atmospheric chemistry model driven by the GEOS-5 assimilated meteorological fields at a horizontal resolution of $1/2^\circ \times 2/3^\circ$. The model used anthropogenic emissions from the Multi-Resolution Emission Inventory of China (MEIC, <http://meicmodel.org>) for the year 2010, except for NH_3 emissions that are taken from the Regional Emission in Asia (REAS-v2) inventory (Kurokawa et al., 2013), with an improved seasonality derived by Zhao et al. (2015). The total NH_3 and NO_x emissions from each source over eastern China and its contribution to total emissions in China are presented in Table S13 in the Supplement. The NH_3 and NO_x emissions over eastern China are 11.6 and 8.5 Tg N yr^{-1} in 2010, which, respectively account for 90 and 89 % of their total emissions over China. Agricultural sources including fertilizer use and livestock comprise most of the NH_3 emissions while fuel combustion activities including industry, power plant, and transportation contribute most of the NO_x emissions and small amounts of NH_3 emissions. Both NH_3 and NO_x have natural sources (including lightning, biomass burning, and soil emissions), but they are negligible compared to anthropogenic emissions over eastern China. Details of the model emissions and mechanisms have been described elsewhere (Zhao et al., 2017; Xu et al., 2018).

We evaluate the model simulations by comparison with measured bulk (both NH_4^+ -N and NO_3^- -N) fluxes. The model biases for bulk NH_4^+ -N and NO_3^- -N deposition were 23 and -23 % respectively (Fig. S13, Supplement). These biases are reasonable, given uncertainties in N_r emissions and predictions of meteorology. Given that model evaluation is not central to this work, we presented the details in Sect. S2 in the Supplement. As shown in Fig. 11, fertilizer use is the dominant source of total N deposition at all sites, with contributions between 16 and 50 %. Also, over eastern China the largest contribution was from fertilizer use (36 %) relative to livestock (10 %), industry (14 %), power plant (11 %), transportation (9 %), and other sources (20 %, the sum of contributions from human waste, residential activities, soil, light-

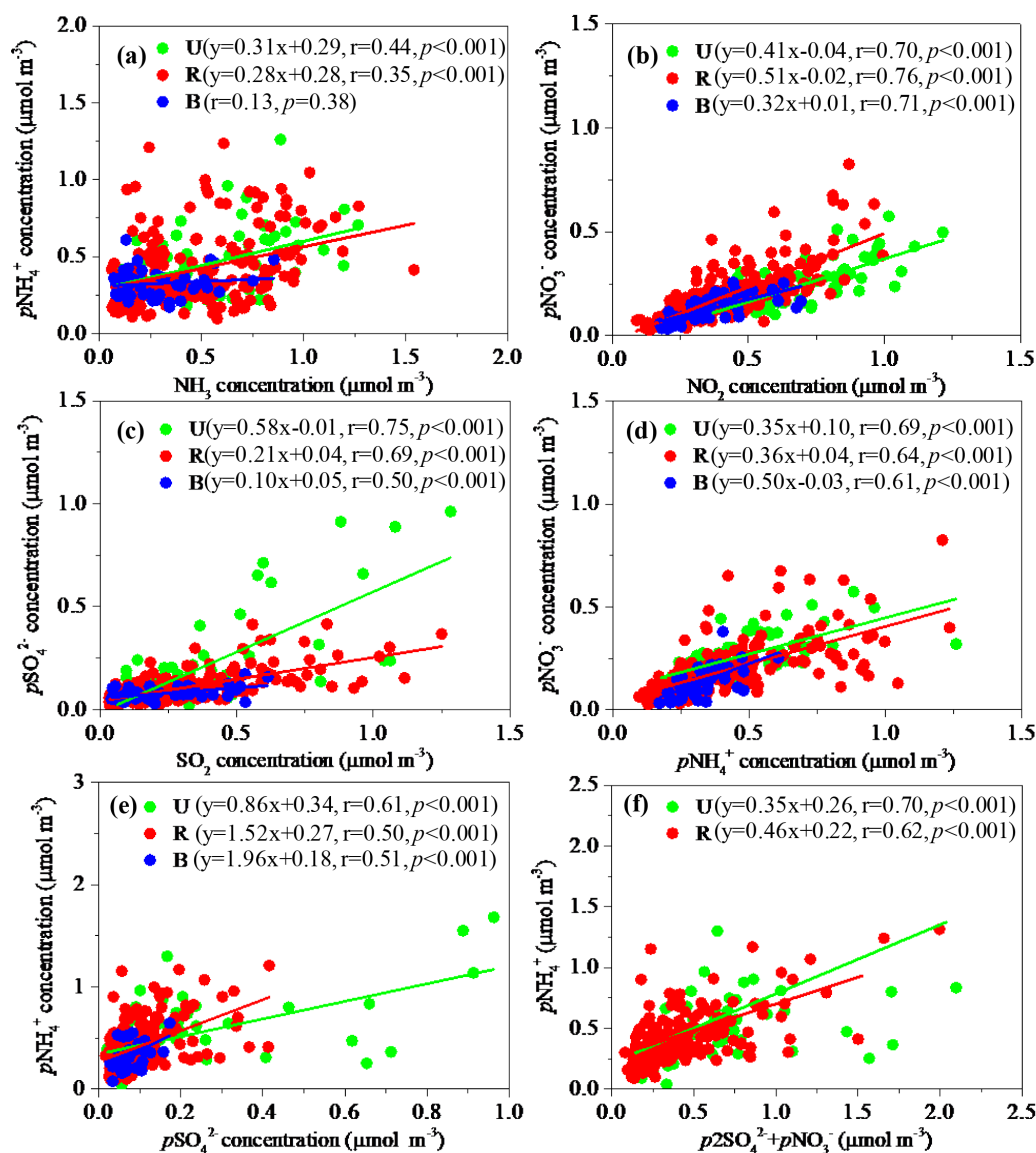


Figure 10. Correlations of monthly mean molar concentrations of (a) $p\text{NH}_4^+$ vs. NH_3 , (b) $p\text{NO}_3^-$ vs. NO_2 , (c) $p\text{SO}_4^{2-}$ vs. SO_2 , (d) $p\text{NO}_3^-$ vs. $p\text{NH}_4^+$, (e) $p\text{NH}_4^+$ vs. $p\text{SO}_4^{2-}$, (f) $p\text{NH}_4^+$ vs. $(p2\text{SO}_4^{2-} + p\text{NO}_3^-)$ at three land use types in eastern China. The number of sites with the same land use type in each region can be found in Table 1.

ing, and biomass burning). These results indicate that reducing NH_3 emissions by use of appropriate fertilization patterns (e.g. 4R technologies: right amount, right time, right form, and right application technique; Ju et al., 2009) should be a priority in curbing N deposition in eastern China. This conclusion to some extent is supported by increased ratios of reduced to oxidized N in the total deposition at three land use types (Fig. 8b), as the major anthropogenic source of reduced N is mainly affected by NH_3 volatilized from animal excrement and the application of nitrogenous fertilizers in agriculture. Absence of NH_3 emission controls may be the main reason for a small and non-significant change in the total N de-

position between 2011–2012 and 2013–2015 (Fig. S6, Supplement), despite enforcement of stringent emission controls on NO_x and SO_2 . To test the importance of future NH_3 emission control strategies, we conducted separate model simulations which reduced NH_3 emissions from fertilizer use by 20%. The results show that a 20% reduction in fertilizer NH_3 emissions can lead to 7.4% decrease in total N deposition over eastern China.

4.5 Deposition response to emission change

Similar to N_f concentrations, there were no significant decreasing trends in dry and bulk deposition of total N or of in-

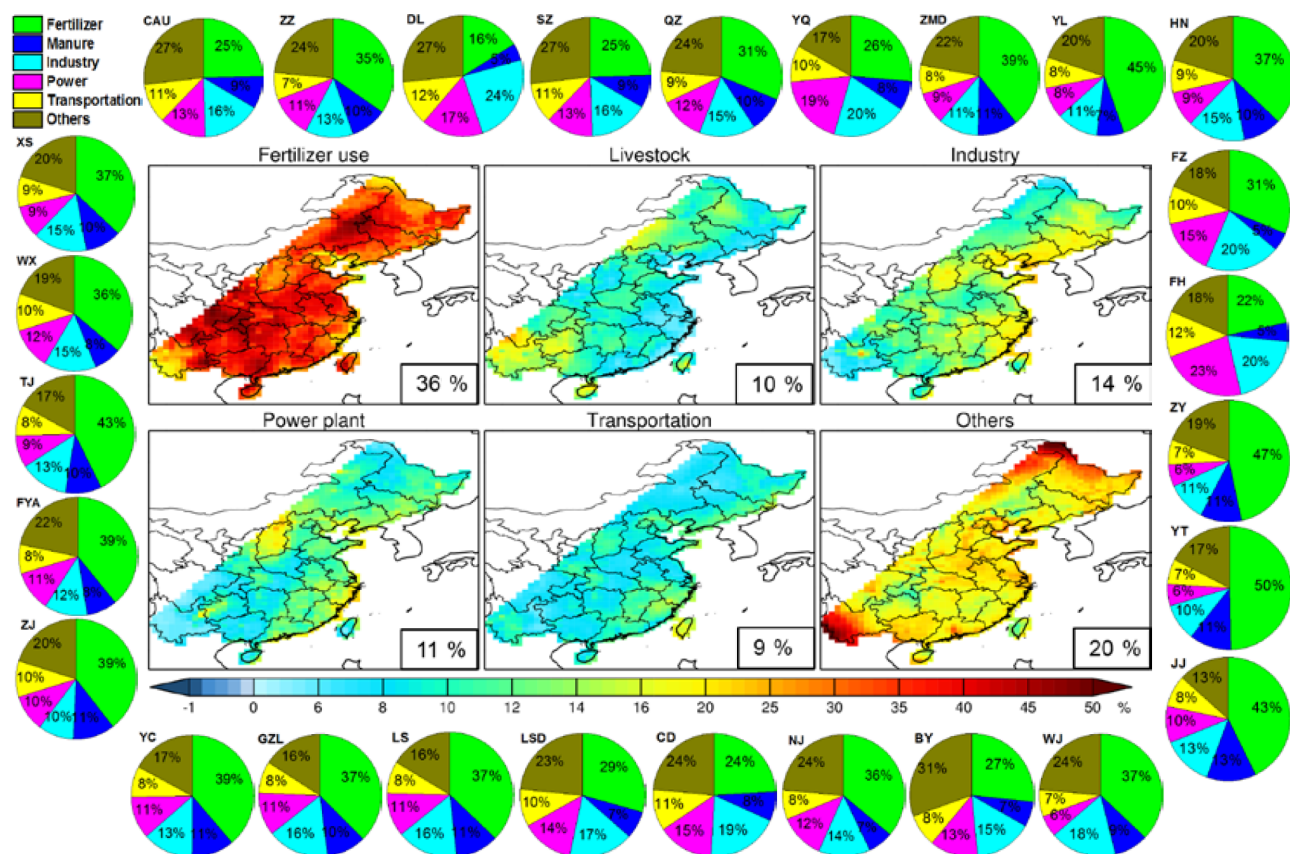


Figure 11. Fractional contributions to total N deposition from emission sectors (i.e. fertilizer use, livestock, industry, power plant, transportation, and others including emissions from human waste, residential activities, soil, lighting, and biomass burning) at the 27 sites and over eastern China.

dividual N_r species at almost all study sites (Figs. S3 and S4, Supplement). In addition, we found that changes in annual mean deposition fluxes of various N_r species are fairly small between the 2013–2015 and 2011–2012 periods (Fig. 5). These results suggest that current emission controls did not effectively reduce N deposition in eastern China.

To further assess the relationship between emission and deposition change, we considered the emissions of SO_2 , NO_x , and NH_3 affecting the 16 study sites with continuous and simultaneous dry and bulk deposition measurements (Fig. S6 and Table S1, Supplement). The regional NH_3 emission data for 2011–2015 were derived from Zhang et al. (2017), while SO_2 and NO_x emission data for 2011–2014 were derived from Xia et al. (2016; emission data for the year 2015 were provided by Yu Zhao, and were unpublished). We compared these annual data with annual mean deposition values from the 16 sites. It should be noted that such assessment is subject to some uncertainty, as emission data were estimated based on the areas belonging to eastern China.

A clear decreasing trend in SO_2 and NO_x emissions was observed, with reductions of 32 and 25 % in 2015 compared to 2011 respectively (Fig. 12a, b). This reduction is directly related to the widespread use of selective catalytic reduction

and flue gas de-sulfurization on power plants and industries (Van der A et al., 2017), and to a lesser extent to the introduction of new emission standards for cars (Liu et al., 2016). In contrast, NH_3 emissions generally showed a gradual increasing trend between 2011 and 2015 (Fig. 12c), as control strategies have not yet been enacted and implemented for NH_3 emissions in China.

Regarding N deposition, a non-significant increasing trend was found for NH_x (slope = $0.36 \text{ kg N ha}^{-1} \text{ yr}^{-1}$) between the 2011 and 2015 period, whereas NO_y deposition exhibited a non-significant decreasing trend (slope = $0.54 \text{ kg N ha}^{-1} \text{ yr}^{-1}$). Also, there were non-significant linear correlations between NH_x deposition and NH_3 emissions and between NO_y deposition and NO_x emissions. This is not surprising given that atmospheric chemistry is complex and often behaves non-linearly (Fowler et al., 2007; Fagerli and Aas, 2008). Interactions between the different pollutants, precipitation variability, and changes in the relative amounts and lifetimes of the chemical species, and in gas–particle partitioning all may contribute to the lack of correlation between emission and deposition trends. Non-linearities between emission and deposition change have been described also elsewhere (Aguillaume et al.,

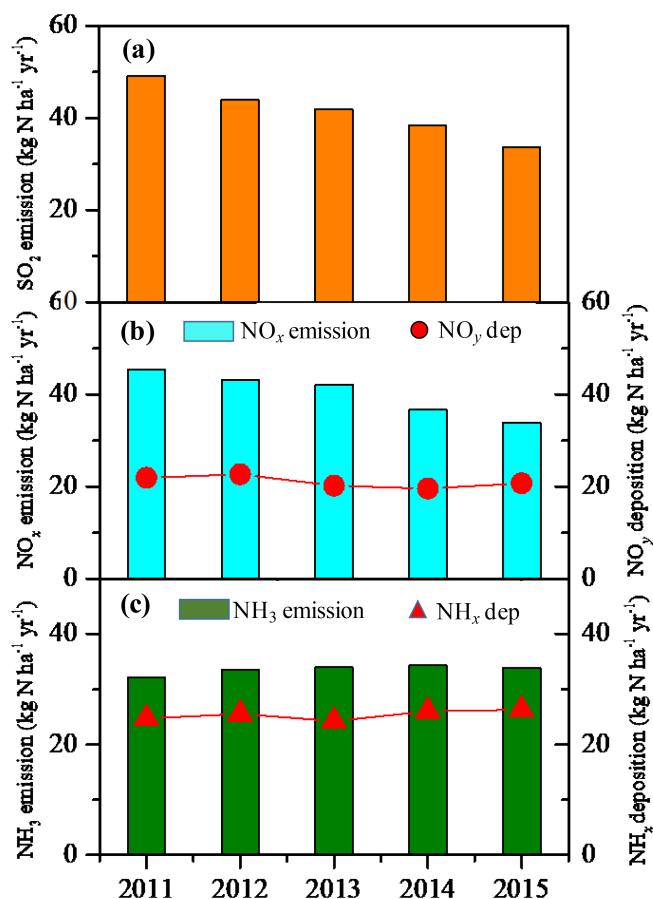


Figure 12. Emissions of SO₂ (a), NO_x (b), and NH₃ (c) obtained as average data from the areas belonging to eastern China, compared with deposition (dep) values in the same periods (mean values from the 16 sites showing in Fig. S6 and Table S1 in the Supplement, 5-year averages).

2016; Karlsson et al., 2011). Deposition in eastern China is also influenced by emissions from outside the region, further degrading any expected correlation with local emissions.

4.6 Uncertainties and limitations

The present study examined annual trends of concentrations of N_r species in air and precipitation as well as dry and bulk N deposition based on Kendall tests and only five annual data values (2011–2015). Although the test can use as few as four data points, indications of statistically significant trends for data sets are unlikely to be truly representative of the trends that are actually occurring due to in the short duration of the measurement data set. Longer time series (e.g. more than 10 years) will likely allow detection of more significant time trends in future work. Another uncertainty may arise from the fact that we used fixed monthly mean dry deposition velocities of gaseous and particulate N_r species for the same months from June 2013 to December 2015. Nevertheless, the uncertainty in the V_d value did not largely af-

fect the deposition trend, as the annual trend in dry deposition of N_r species is more likely driven by changes in ambient N_r concentrations than by changing deposition velocities, as evident from fairly low standard deviations of annual mean V_d of N_r species at our selected 27 sites between 2008 and 2012 (~0.029 for NH₃, ~0.005 for NO₂, ~0.054 for HNO₃, and ~0.019 for both pNH₄⁺ and pNO₃⁻; data were extracted from Zhao et al., 2017).

In addition, we did not account for inter-annual changes in meteorology, which also strongly influences atmospheric N_r levels and N deposition (Xu et al., 2015, 2017). For example, air concentrations of NO₂, NH₃, pNH₄⁺, and pNO₃⁻ tend to increase under the relatively stagnant conditions prior to a cold front's arrival and decrease substantially after the cold front brings precipitation and strong winds into the region (Xu et al., 2017). On the inter-annual timescale, the frequency of cold front passage may be affected by large-scale circulation patterns such as the position of the Siberian High for eastern China (Jia et al., 2015). For example, a large inter-annual variation in precipitation amount was observed at the selected 16 sites during 2011–2015 (Fig. S14, Supplement), which partially lead to inter-annual changes in wet/bulk N deposition. However, given that in situ measurements of other meteorological variables (e.g. air temperature, relative humidity, air pressure, wind speed and direction) are not available, and that GEOS-5 assimilated meteorological fields were updated after May 2013, an evaluation of the effect of meteorology on N_r concentration and deposition is recommended for future work.

Uncertainties also exist in the source attribution calculated with the GEOS-Chem simulations, since results largely depend on the emission inventories fed to the model. Zhao et al. (2017) pointed out that uncertainties in current NH₃ emissions inventories (e.g. large range of emission values in current studies and absence of bi-directional NH₃ exchange between the land and atmosphere) may influence nitrogen deposition simulation in China. Future work based on improved NH₃ emission inventories (e.g. Zhang et al., 2018) and including bidirectional ammonia exchange with the surface is essential to better examine source attribution of N deposition in China.

5 Conclusion

We have characterized spatial and temporal (annual and seasonal) variations in concentrations and deposition of major N_r species in air (NH₃, NO₂, HNO₃, pNH₄⁺, and pNO₃⁻) and precipitation (NH₄⁺-N and NO₃⁻-N) for three land use types (e.g. urban, rural, and background) in eastern China by examining 5-year (2011–2015) in situ measurements at 27 sites. We further examined regional features of N_r pollution by comparison of satellite and surface measurements of NH₃ and NO₂ and examined the sources of total N deposition over the whole region for the year 2010 using the GEOS-Chem

model at horizontal resolution of $1/2^\circ \times 2/3^\circ$. Our major results and conclusions are as follows.

In eastern China, annual mean concentrations and dry and bulk deposition fluxes of measured N_r species in air and precipitation generally ranked in the order urban > rural > background. The air concentrations and dry deposition were usually higher at all land use types in the northern region of eastern China than in the southern region, especially (except HNO_3) at rural sites, for which the differences reached statistically significant levels. This is also true for the annual VWM concentrations of NH_4^+ -N, NO_3^- -N, and TIN in precipitation, whereas bulk deposition fluxes of these species were comparable for matched land use types between the northern and southern regions.

No significant trends in the annual mean concentrations and dry and bulk deposition fluxes of measured N_r species in air and precipitation were observed at almost all sites during the 2011–2015 period. Also, annual averages of these values showed non-significant changes between the 2011–2012 and 2013–2015 periods for all land use types. Ambient total concentrations of measured N_r species showed a non-significant seasonal variation at all land use types, whereas individual N_r species exhibited a significant seasonal variation in most cases, except for NO_2 and pNH_4^+ at urban sites, and HNO_3 at all land use types. Unlike air concentrations, dry deposition of total N_r showed consistent and significant seasonal variation for each land use type, with the highest values in summer and the lowest values in winter. The V_d was a dominant factor influencing seasonal variations of NO_2 , HNO_3 , and pNH_4^+ concentrations, while seasonal variations of NH_3 and pNO_3^- are mainly influenced by their respective air concentrations. The concentrations of NH_4^+ -N, NO_3^- -N, and TIN in precipitation showed significant seasonal variations, ranking in the consistent order of winter > spring > autumn \approx summer. Also, significant seasonal variations in bulk deposition were also found, following the consistent order of summer > spring \approx autumn > winter.

Both IASI satellite-retrieved NH_3 columns and OMI satellite-retrieved NO_2 columns over eastern China showed higher values in the north than in the south. In addition, significant positive correlations were found between measured NH_3 concentrations and retrieved NH_3 columns, and between measured NO_2 concentrations and columns. These results together reveal that atmospheric N_r pollution is more serious in the northern region, and also suggest that satellite retrievals of NH_3 and NO_2 columns can provide useful information on spatial concentration variability of these two key N_r species at a regional or national scale. Weak correlations between IASI_ NH_3 observations and surface NH_3 measurements were found at most selected sites, suggesting that IASI_ NH_3 observations in their current state are not as readily used to accurately track temporal variability in surface NH_3 concentrations.

Ammonia is currently not included in China's emission control policies of air pollution precursors, although the ne-

cessity of mitigation has been the subject of discussion during recent years. Across all urban and rural sites, the slopes of the regression relation between pNH_4^+ and the sum of pSO_4^{2-} and pNO_3^- were both smaller than unity, indicating that controlling NH_3 emissions not only can directly reduce ambient NH_3 concentrations, but also lower the formation of pNH_4^+ and pNO_3^- . Fertilizer use contributed 36 % of the total N deposition over eastern China, suggesting reducing NH_3 emissions from fertilizer application would be an effective strategy for reducing N deposition. Overall, our findings reveal persistent serious N_r pollution during the 12th FYP period despite implementation of current emission controls, and highlight the importance of NH_3 emission controls for mitigating future atmospheric N_r concentrations and deposition in eastern China.

Data availability. The data used in this study are available from the corresponding author upon request (liu310@cau.edu.cn).

The Supplement related to this article is available online at <https://doi.org/10.5194/acp-18-10931-2018-supplement>.

Author contributions. XJL, FZ, and WX designed the research; WX, XSL, JS, and LLu conducted the field work; LLi, XZ, and MC prepared IASI_ NH_3 and OMI_ NO_2 products; YHZ and LZ conducted model simulations; XZ and BG provided the ammonia emission data; YZ provided the emission data of nitrogen dioxide and sulfur dioxide; WX, LLi, MC, YL, and YHZ performed the data analysis and prepared the figures and tables; WX and XJL wrote the paper with comments from JLC, ZF, and YP.

Competing interests. The authors declare that they have no conflict of interest.

Acknowledgements. This study was supported by the National Key R&D Program of China (2017YFC0210101, 2017YFC0210106, 2014BC954202), the National Natural Science Foundation of China (41705130, 41425007, 31421092) as well as the National Ten-thousand Talents Program of China (Xuejun Liu). The authors thank all staff at the study sites (listed in Table S1, Supplement) for their cooperation during sample collection. We also thank two anonymous reviewers for insightful comments regarding the improvement of the paper.

Leiming Zhang
Reviewed by: two anonymous referees

References

Aguillaume, L., Rodrigo, A., and Avila, A.: Long-term effects of changing atmospheric pollution on throughfall, bulk deposition

- and streamwaters in a Mediterranean forest, *Sci. Total Environ.*, 544, 919–928, <https://doi.org/10.1016/j.scitotenv.2015.12.017>, 2016.
- Allen, A. G., Harrison, R. M., and Erisman, J. W.: Field measurements of the dissociation of ammonium nitrate and ammonium chloride aerosols, *Atmos. Environ.*, 23, 1591–1599, 1989.
- Atkins, D. H. F. and Lee, D. S.: Spatial and temporal variation of rural nitrogen dioxide concentrations across the United Kingdom, *Atmos. Environ.*, 29, 223–239, 1995.
- Bobbink, R., Hicks, K., Galloway, J., Spranger, T., Alkemade, R., Ashmore, M., Bustamante, M., Cinderby, S., Davidson, E., and Dentener, F.: Global assessment of nitrogen deposition effects on terrestrial plant diversity: a synthesis, *Ecol. Appl.*, 20, 30–59, 2010.
- Boersma, K. F., Eskes, H. J., Veeffkind, J. P., Brinkma, E. J., van der A, R. J., Sneep, M., van den Oord, G. H. J., Levelt, P. F., Stammes, P., Gleason, J. F., and Bucsele, E. J.: Near-real time retrieval of tropospheric NO₂ from OMI, *Atmos. Chem. Phys.*, 7, 2103–2118, <https://doi.org/10.5194/acp-7-2103-2007>, 2007.
- Cao, J. J., Zhang, T., Chow, J. C., Watson, J. G., Wu, F., and Li, H.: Characterization of atmospheric ammonia over Xi'an, China, *Aerosol Air Qual. Res.*, 9, 277–289, 2009.
- Chang, Y. H., Liu, X. J., Deng, C. R., Dore, A. J., and Zhuang, G. S.: Source apportionment of atmospheric ammonia before, during, and after the 2014 APEC summit in Beijing using stable nitrogen isotope signatures, *Atmos. Chem. Phys.*, 16, 11635–11647, <https://doi.org/10.5194/acp-16-11635-2016>, 2016.
- Dammers, E., Palm, M., Van Damme, M., Vigouroux, C., Smale, D., Conway, S., Toon, G. C., Jones, N., Nussbaumer, E., Warneke, T., Petri, C., Clarisse, L., Clerbaux, C., Hermans, C., Lutsch, E., Strong, K., Hannigan, J. W., Nakajima, H., Morino, I., Herrera, B., Stremme, W., Grutter, M., Schaap, M., Wichink Kruit, R. J., Notholt, J., Coheur, P. F., and Erisman, J. W.: An evaluation of IASI-NH₃ with ground-based Fourier transform infrared spectroscopy measurements, *Atmos. Chem. Phys.*, 16, 10351–10368, <https://doi.org/10.5194/acp-16-10351-2016>, 2016.
- Erisman, J. W., Grennfelt, P., and Sutton, M.: The European perspective on nitrogen emission and deposition, *Environ. Int.*, 29, 311–325, [https://doi.org/10.1016/S0160-4120\(02\)00162-9](https://doi.org/10.1016/S0160-4120(02)00162-9), 2003.
- Fagerli, H. and Aas, W.: Trends of nitrogen in air and precipitation: model results and observations at EMEP sites in Europe, 1980–2003, *Environ. Pollut.*, 154, 448–461, <https://doi.org/10.1016/j.envpol.2008.01.024>, 2008.
- Fenn, M. E., Baron, J. S., Allen, E. B., Rueth, H. M., Nydick, K. R., Geiser, L., Bowman, W. D., Sickman, J. O., Meixner, T., Johnson, D. W., and Neitlich, P.: Ecological Effects of Nitrogen Deposition in the Western United States, *BioScience*, 53, 404–420, [https://doi.org/10.1641/0006-3568\(2003\)053\[0404:EEONDI\]2.0.CO;2](https://doi.org/10.1641/0006-3568(2003)053[0404:EEONDI]2.0.CO;2), 2003.
- Fowler, D., Smith, R., Muller, J., Cape, J. N., Sutton, M., Erisman, J. W., and Fagerli, H.: Long term trends in sulphur and nitrogen deposition in Europe and the cause of non-linearities, *Water Air Soil Pollut.*, 7, 41–47, <https://doi.org/10.1007/s11267-006-9102-x>, 2007.
- Fowler, D., Coyle, M., Skiba, U., Sutton, M. A., Cape, J. N., Reis, S., Sheppard, L. J., Jenkins, A., Grizzetti, B., Galloway, J. N., Vitousek, P., Leach, A., Bouwman, A. F., Butterbach-Bahl, K., Dentener, F., Stevenson, D., Amann, M., and Voss, M.: The global nitrogen cycle in the twenty-first century, *Philos. T. R. Soc. B*, 368, 20130164, <https://doi.org/10.1098/rstb.2013.0164>, 2013.
- Fuzzi, S., Baltensperger, U., Carslaw, K., Decesari, S., van Der Gon, H. D., Facchini, M. C., Fowler, D., Koren, I., Langford, B., Lohmann, U., Nemitz, E., Pandis, S., Riipinen, I., Rudich, Y., Schaap, M., Slowik, J. G., Spracklen, D. V., Vignati, E., Wild, M., Williams, M., and Gilardoni, S.: Particulate matter, air quality and climate: lessons learned and future needs, *Atmos. Chem. Phys.*, 15, 8217–8299, <https://doi.org/10.5194/acp-15-8217-2015>, 2015.
- Galloway, J. N., Townsend, A. R., Erisman, J. W., Bekunda, M., Cai, Z., Freney, J. R., Martinelli, L. A., Seitzinger, S. P., and Sutton, M. A.: Transformation of the Nitrogen Cycle: Recent trends, questions, and potential solutions, *Science*, 320, 889–892, <https://doi.org/10.1126/science.1136674>, 2008.
- Ge, B. Z., Wang, Z. F., Xu, X. B., Wu, J. B., Yu, X. L., and Li, J.: Wet deposition of acidifying substances in different regions of China and the rest of East Asia: modeling with updated NAQPMS, *Environ. Pollut.*, 187, 10–21, <https://doi.org/10.1016/j.envpol.2013.12.014>, 2014.
- Gilbert, R. O.: Statistical methods for environmental pollution monitoring, John Wiley & Sons, 1987.
- Gu, B. J., Sutton, M. A., Chang, S. X., Ge, Y., and Jie, C.: Agricultural ammonia emissions contribute to China's urban air pollution, *Front. Ecol. Environ.*, 12, 265–266, <https://doi.org/10.1890/14.WB.007>, 2014.
- Guo, S., Hu, M., Zamora, M. L., Peng, J. F., Shang, D. J., Zheng, J., Du, Z. F., Wu, Z. J., Shao, M., and Zeng, L. M.: Elucidating severe urban haze formation in China, *P. Natl. Acad. Sci. USA*, 111, 17373, <https://doi.org/10.1073/pnas.1419604111>, 2014.
- Han, X., Zhang, M. G., Skorokhod, A., and Kou, X. X.: Modeling dry deposition of reactive nitrogen in China with RAMS-CMAQ, *Atmos. Environ.*, 166, 47–61, <https://doi.org/10.1016/j.atmosenv.2017.07.015>, 2017.
- He, N. P., Zhu, J. X., and Wang, Q. F.: Uncertainty and perspectives in studies of atmospheric nitrogen deposition in China: A response to Liu et al. (2015), *Sci. Total Environ.*, 520, 302–304, <https://doi.org/10.1016/j.scitotenv.2015.03.063>, 2015.
- Huang, P., Zhang, J. B., Xin, X. L., Zhu, A. N., Zhang, C. Z., Ma, D. H., Zhu, Q. G., Yang, S., and Wu, S. J.: Proton accumulation accelerated by heavy chemical nitrogen fertilization and its long-term impact on acidifying rate in a typical arable soil in the Huang-Huai-Hai Plain, *J. Integr. Agric.*, 14, 148–157, 2015.
- Huang, R. J., Zhang, Y., Bozzetti, C., Ho, K. F., Cao, J. J., Han, Y., Daellenbach, K. R., Slowik, J. G., Platt, S. M., Canonaco, F., Zotter, P., Wolf, R., Pieber, S. M., Bruns, E. A., Crippa, M., Ciarelli, G., Piazzalunga, A., Schwikowski, M., Abbaszade, G., Schnelle-Kreis, J., Zimmermann, R., An, Z., Szidat, S., Baltensperger, U., El Haddad, I., and Prevot, A. S.: High secondary aerosol contribution to particulate pollution during haze events in China, *Nature*, 514, 218–222, <https://doi.org/10.1038/nature13774>, 2014.
- Huang, X., Song, Y., Li, M. M., Li, J. F., Huo, Q., Cai, X. H., Zhu, T., Hu, M., and Zhang, H. S.: A high-resolution ammonia emission inventory in China, *Global Biogeochem. Cy.*, 26, GB1030, <https://doi.org/10.1029/2011GB004161>, 2012.
- Ianniello, A., Spataro, F., Esposito, G., Allegrini, I., Rantica, E., Ancora, M. P., Hu, M., and Zhu, T.: Occurrence of gas phase

- ammonia in the area of Beijing (China), *Atmos. Chem. Phys.*, 10, 9487–9503, <https://doi.org/10.5194/acp-10-9487-2010>, 2010.
- Jia, B., Wang, Y., Yao, Y., and Xie, Y.: A new indicator on the impact of large-scale circulation on wintertime particulate matter pollution over China, *Atmos. Chem. Phys.*, 15, 11919–11929, <https://doi.org/10.5194/acp-15-11919-2015>, 2015.
- Jia, Y. L., Yu, G. R., He, N. P., Zhan, X. Y., Fang, H. J., Sheng, W. P., Zuo, Y., Zhang, D. Y., and Wang, Q. F.: Spatial and decadal variations in inorganic nitrogen wet deposition in China induced by human activity, *Sci. Rep.*, 4, 3763, <https://doi.org/10.1038/srep03763>, 2014.
- Jia, Y. L., Yu, G. R., Gao, Y. N., He, N. P., Wang, Q. F., Jiao, C. C., and Zuo, Y.: Global inorganic nitrogen dry deposition inferred from ground and space-based measurements, *Sci. Rep.*, 6, 19810, <https://doi.org/10.1038/srep19810>, 2016.
- Ju, X. T., Xing, G. X., Chen, X. P., Zhang, S. L., Zhang, L. J., Liu, X. J., Cui, Z. L., Yin, B., Christie, P., Zhu, Z. L., and Zhang, F. S.: Reducing environmental risk by improving N management in intensive Chinese agricultural systems, *P. Natl. Acad. Sci. USA*, 106, 3041–3046, <https://doi.org/10.1073/pnas.0902655106>, 2009.
- Kanakidou, M., Myriokefalitakis, S., Daskalakis, N., and Fanourgakis, G.: Past, present, and future atmospheric nitrogen deposition, *J. Atmos. Sci.*, 73, 160303130433005, <https://doi.org/10.1175/JAS-D-15-0278.s1>, 2016.
- Karlsson, G. P., Akselsson, C., Hellsten, S., and Karlsson, P. E.: Reduced European emissions of S and N effects on air concentrations, deposition and soil water chemistry in Swedish forests, *Environ. Pollut.* 159, 3571–3582, <https://doi.org/10.1016/j.envpol.2011.08.007>, 2011.
- Khoder, M. I.: Atmospheric conversion of sulfur dioxide to particulate sulfate and nitrogen dioxide to particulate nitrate and gaseous nitric acid in an urban area, *Chemosphere*, 49, 675–684, 2002.
- Krotkov, N. A., Mclinden, C. A., Li, C., Lamsal, L. N., Celarier, E. A., Marchenko, S. V., Swartz, W. H., Bucsela, E. J., Joiner, J., Duncan, B. N., Boersma, K. F., Veeffkind, J. P., Levelt, P. F., Fioletov, V. E., Dickerson, R. R., He, H., Lu, Z. F., and Streets, D. G.: Aura OMI observations of regional SO₂ and NO₂ pollution changes from 2005 to 2015, *Atmos. Chem. Phys.*, 16, 4605–4629, <https://doi.org/10.5194/acp-16-4605-2016>, 2016.
- Kurokawa, J., Ohara, T., Morikawa, T., Hanayama, S., Janssens-Maenhout, G., Fukui, T., Kawashima, K., and Akimoto, H.: Emissions of air pollutants and greenhouse gases over Asian regions during 2000–2008: Regional Emission inventory in Asia (REAS) version 2, *Atmos. Chem. Phys.*, 13, 11019–11058, <https://doi.org/10.5194/acp-13-11019-2013>, 2013.
- Li, H., Zhang, Q., Zheng, B., Chen, C., Wu, N., Guo, H., Zhang, Y., Zheng, Y., Li, X., and He, K.: Nitrate-driven urban haze pollution during summertime over the North China Plain, *Atmos. Chem. Phys.*, 18, 5293–5306, <https://doi.org/10.5194/acp-18-5293-2018>, 2018.
- Li, Y., Niu, S., and Yu, G.: Aggravated phosphorus limitation on biomass production under increasing nitrogen loading: a meta-analysis, *Global Change Biol.*, 22, 934–943, <https://doi.org/10.1111/gcb.13125>, 2016.
- Liang, X., Zou, T., Guo, B., Li, S., Zhang, H. Z., Zhang, S. Y., Huang, H., and Chen, S. X.: Assessing Beijing’s PM_{2.5} pollution: severity, weather impact, APEC and winter heating, *Proc. R. Soc. A*, 471, 20150257, <https://doi.org/10.1098/rspa.2015.0257>, 2015.
- Liu, F., Beirle, S., Zhang, Q., van der A, R. J., Zheng, B., Tong, D., and He, K.: NO_x emission trends over Chinese cities estimated from OMI observations during 2005 to 2015, *Atmos. Chem. Phys.*, 17, 9261–9275, <https://doi.org/10.5194/acp-17-9261-2017>, 2017.
- Liu, L., Zhang, X. Y., Zhang, Y., Xu, W., Liu, X. J., Zhang, X. M., Feng, J. L., Chen, X. R., Zhang, Y. H., Lu, X. H., Wang, S. Q., Zhang, W. T., and Zhao, L. M.: Dry particulate nitrate deposition in China, *Environ. Sci. Technol.*, 51, 5572, <https://doi.org/10.1021/acs.est.7b00898>, 2017a.
- Liu, L., Zhang, X., Xu, W., Liu, X., Li, Y., Lu, X., Zhang, Y., and Zhang, W.: Temporal characteristics of atmospheric ammonia and nitrogen dioxide over China based on emission data, satellite observations and atmospheric transport modeling since 1980, *Atmos. Chem. Phys.*, 17, 9365–9378, <https://doi.org/10.5194/acp-17-9365-2017>, 2017b.
- Liu, X. J., Duan, L., Mo, J. M., Du, E. Z., Shen, J. L., Lu, X. K., Zhang, Y., Zhou, X. B., He, C. E., and Zhang, F. S.: Nitrogen deposition and its ecological impact in China: An overview, *Environ. Pollut.*, 159, 2251–2264, <https://doi.org/10.1016/j.envpol.2010.08.002>, 2011.
- Liu, X. J., Zhang, Y., Han, W. X., Tang, A., Shen, J. L., Cui, Z. L., Vitousek, P., Erisman, J. W., Goulding, K., Christie, P., Fangmeier, A., and Zhang, F. S.: Enhanced nitrogen deposition over China, *Nature*, 494, 459–462, <https://doi.org/10.1038/nature11917>, 2013.
- Liu, X. J., Vitousek, P., Chang, Y. H., Zhang, W. F., Matson, P., and Zhang, F. S.: Evidence for a historic change occurring in China, *Environ. Sci. Technol.*, 50, 505–506, <https://doi.org/10.1021/acs.est.5b05972>, 2016.
- Lu, C. Q. and Tian, H. Q.: Spatial and temporal patterns of nitrogen deposition in China: Synthesis of observational data, *J. Geophys. Res.*, 112, D22S05, <https://doi.org/10.1029/2006JD007990>, 2007.
- Lu, C. Q. and Tian, H. Q.: Half-century nitrogen deposition increase across China: A gridded time-series data set for regional environmental assessments, *Atmos. Environ.*, 97, 68–74, <https://doi.org/10.1016/j.atmosenv.2014.07.061>, 2014.
- Marchetto, A., Rogora, M., and Arisci, S.: Trend analysis of atmospheric deposition data: A comparison of statistical approaches, *Atmos. Environ.*, 64, 95–102, 2013.
- Meng, Z. Y., Xu, X. B., Wang, T., Zhang, X. Y., Yu, X. L., Wang, S. F., Lin, W. L., Chen, Y. Z., Jiang, Y. A., and An, X. Q.: Ambient sulfur dioxide, nitrogen dioxide, and ammonia at ten background and rural sites in China during 2007–2008, *Atmos. Environ.*, 44, 2625–2631, 2008.
- Meng, Z. Y., Xu, X. B., Lin, W. L., Ge, B. Z., Xie, Y. L., Song, B., Jia, S. H., Zhang, R., Peng, W., Wang, Y., Cheng, H. B., Yang, W., and Zhao, H.: Role of ambient ammonia in particulate ammonium formation at a rural site in the North China Plain, *Atmos. Chem. Phys.*, 18, 167–184, <https://doi.org/10.5194/acp-18-167-2018>, 2018.
- MEPC (Ministry of Environmental Protection of the People’s Republic of China): Report on Environmental Quality in China, 2010, available at: http://jcs.mep.gov.cn/hjzl/zkgb/2010zkgb/201106/t20110602_211579.htm, last access: 3 June 2011.
- Miyazaki, K., Eskes, H., Sudo, K., Boersma, K. F., Bowman, K., and Kanaya, Y.: Decadal changes in global surface NO_x emissions from multi-constituent satellite data assimilation, *Atmos.*

- Chem. Phys., 17, 807–837, <https://doi.org/10.5194/acp-17-807-2017>, 2017.
- Pan, Y. P., Wang, Y. S., Tang, G. Q., and Wu, D.: Wet and dry deposition of atmospheric nitrogen at ten sites in Northern China, *Atmos. Chem. Phys.*, 12, 6515–6535, <https://doi.org/10.5194/acp-12-6515-2012>, 2012.
- Pan, Y. P., Wang, Y. S., Zhang, J. K., Liu, Z. R., Wang, L. L., Tian, S. L., Tang, G. Q., Gao, W. K., Ji, D. S., and Song, T.: Redefining the importance of nitrate during haze pollution to help optimize an emission control strategy, *Atmos. Environ.*, 141, 197–202, <https://doi.org/10.1016/j.atmosenv.2016.06.035>, 2016.
- Pinder, R. W., Walker, J. T., Bash, J. O., Cady-Pereira, K. E., Henze, D. K., Luo, M. Z., Osterman, G. B., and Shephard, M. W.: Quantifying spatial and seasonal variability in atmospheric ammonia with in situ and space-based observations, *Geophys. Res. Lett.*, 38, L04802, <https://doi.org/10.1029/2010GL046146>, 2011.
- Russell, A. R., Valin, L. C., and Cohen, R. C.: Trends in OMI NO₂ observations over the United States: effects of emission control technology and the economic recession, *Atmos. Chem. Phys.*, 12, 12197–12209, <https://doi.org/10.5194/acp-12-12197-2012>, 2012.
- Salmi, T., Maatta, A., Anttila, P., Ruoho-Airola, T., and Amnell, T.: Detecting trends of annual values of atmospheric pollutants by the Mann–Kendall test and Sen’s slope estimates – the Excel template application MAKESENS. Publications on Air Quality No. 31, Finnish Meteorological Institute, Helsinki, Finland, 2002.
- Seinfeld, J. H. and Pandis, S. N.: *Atmospheric chemistry and physics: from air pollution to climate change*, 2nd Edn., Wiley Interscience, New Jersey, 2006.
- She, W.: Hu Huanyong: father of China’s population geography, *China Popul. Today*, 15, 1–20, 1998.
- Souri, A. H., Choi, Y., Jeon, W., Woo, J.-H., Zhang, Q., and Kurokawa, J.-i.: Remote sensing evidence of decadal changes in major tropospheric ozone precursors over East Asia, *J. Geophys. Res.*, 122, 2474–2492, <https://doi.org/10.1002/2016JD025663>, 2017.
- Tang, Y. S., Simmons, I., van Dijk, N., Di Marco, C., Nemitz, E., Damme, U., Gilke, K., Djuricic, V., Vidic, S., and Gliha, Z.: European scale application of atmospheric reactive nitrogen measurements in a low-cost approach to infer dry deposition fluxes, *Agr. Ecosyst. Environ.*, 133, 183–195, <https://doi.org/10.1016/j.agee.2009.04.027>, 2009.
- Theil, H.: A Rank-Invariant Method of Linear and Polynomial Regression Analysis, in: *Henri Theil’s Contributions to Economics and Econometrics*, edited by: Raj, B. and Koerts, J., *Advanced Studies in Theoretical and Applied Econometrics*, Springer Netherlands, 345–381, 1992.
- Tian, S. L., Pan, Y. P., Liu, Z. R., Wen, T. X., and Wang, Y. S.: Size-resolved aerosol chemical analysis of extreme haze pollution events during early 2013 in urban Beijing, China, *J. Hazard. Mater.*, 279, 452–460, <https://doi.org/10.1016/j.jhazmat.2014.07.023>, 2014.
- Van Damme, M., Clarisse, L., Dammers, E., Liu, X., Nowak, J. B., Clerbaux, C., Flechard, C. R., Galy-lacaux, C., Xu, W., and Neuman, J. A.: Towards validation of ammonia (NH₃) measurements from the IASI satellite, *Atmos. Meas. Tech.*, 8, 1575–1591, <https://doi.org/10.5194/amt-8-1575-2015>, 2015.
- van der A, R. J., Mijling, B., Ding, J., Koukouli, M. E., Liu, F., Li, Q., Mao, H., and Theys, N.: Cleaning up the air: effectiveness of air quality policy for SO₂ and NO_x emissions in China, *Atmos. Chem. Phys.*, 17, 1775–1789, <https://doi.org/10.5194/acp-17-1775-2017>, 2017.
- Vet, R., Artz, R. S., Carou, S., Shaw, M., Ro, C.-U., Aas, W., Baker, A., Bowersox, V. C., Dentener, F., Galy-Lacaux, C., Hou, A., Pienaar, J. J., Gillett, R., Forti, M. C., Gromov, S., Hara, H., Khodzher, T., Mahowald, N. M., Nickovic, S., Rao, P. S. P., and Reid, N. W.: A global assessment of precipitation chemistry and deposition of sulfur, nitrogen, sea salt, base cations, organic acids, acidity and pH, and phosphorus, *Atmos. Environ.*, 93, 3–100, <https://doi.org/10.1016/j.atmosenv.2013.10.060>, 2014.
- Walker, J. T., Whittall, D. R., Robarge, W., and Paerl, H. W.: Ambient ammonia and ammonium aerosol across a region of variable ammonia emission density, *Atmos. Environ.*, 38, 1235–1246, 2004.
- Wang, G. H., Zhang, R. Y., Gomez, M. E., Yang, L. X., Zamora, M. L., Hu, M., Lin, Y., Peng J. F., Guo, S., Meng, J. J., Li, J. J., Cheng, C. L., Hu, T. F., Ren, Y. Q., Wang, Y. S., Gao, J., Cao, J. J., An, Z. S., Zhou, W. J., Li, G. H., Wang, J. Y., Tian, P. F., Marrero-Ortiz, W., Secrest J., Du, Z. F., Zheng, J., Shang, D. J., Zeng, L. M., Shao, M., Wang, W. G., Huang, Y., Wang, Y., Zhu, Y. J., Li, Y. X., Hu, J. X., Pan, B. W., Cai, L., Cheng, Y. T., Ji, Y. M., Zhang, F., Rosenfeld, D., Liss, P. S., Duce, R. A., Kolb, C. E., and Molina, M. J.: Persistent sulfate formation from London Fog to Chinese haze, *P. Natl. Acad. Sci. USA*, 113, 13630, <https://doi.org/10.1073/pnas.1616540113>, 2016.
- Wang, S. X., Xing, J., Jang, C. R., Zhu, Y., Fu, J. S., and Hao, J. M.: Impact assessment of ammonia emissions on inorganic aerosols in East China using response surface modeling technique, *Environ. Sci. Technol.*, 45, 9293–9300, <https://doi.org/10.1021/es2022347>, 2011.
- Wen, L., Chen, J. M., Yang, L. X., Wang, X. F., Xu, C. H., Sui, X., Yao, L., Zhu, Y. H., Zhang, J. M., Zhu, T., and Wang, W. X.: Enhanced formation of fine particulate nitrate at a rural site on the North China Plain in summer: The important roles of ammonia and ozone, *Atmos. Environ.*, 101, 294–302, <https://doi.org/10.1016/j.atmosenv.2014.11.037>, 2015.
- Wesely, M. L.: Parameterization of surface resistances to gaseous dry deposition in regional-scale numerical-models, *Atmos. Environ.*, 23, 1293–1304, 1989.
- Whitburn, S., Van Damme, M., Clarisse, L., Bauduin, S., Heald, C. L., Hadji-Lazaro, J., Hurtmans, D., Zondlo, M. A., Clerbaux, C., and Coheur, P. F.: A flexible and robust neural network IASINH3 retrieval algorithm, *J. Geophys. Res.-Atmos.*, 121, 6581–6599, <https://doi.org/10.1002/2016JD024828>, 2016.
- Xia, Y. M., Zhao, Y., and Nielsen, C. P.: Benefits of China’s efforts in gaseous pollutant control indicated by the bottom-up emissions and satellite observations 2000–2014, *Atmos. Environ.*, 136, 43–53, <https://doi.org/10.1016/j.atmosenv.2016.04.013>, 2016.
- Xu, W., Luo, X. S., Pan, Y. P., Zhang, L., Tang, A. H., Shen, J. L., Zhang, Y., Li, K. H., Wu, Q. H., Yang, D. W., Zhang, Y. Y., Xue, J., Li, W. Q., Li, Q. Q., Tang, L., Lu, S. H., Liang, T., Tong, Y. A., Liu, P., Zhang, Q., Xiong, Z. Q., Shi, X. J., Wu, L. H., Shi, W. Q., Tian, K., Zhong, X. H., Shi, K., Tang, Q. Y., Zhang, L. J., Huang, J. L., He, C. E., Kuang, F. H., Zhu, B., Liu, H., Jin, X., Xin, Y. J., Shi, X. K., Du, E. Z., Dore, A. J., Tang, S., Collett Jr., J. L., Goulding, K., Sun, Y. X., Ren, J., Zhang, F. S., and Liu, X. J.: Quantifying atmospheric nitrogen deposition through

- a nationwide monitoring network across China, *Atmos. Chem. Phys.*, 15, 12345–12360, <https://doi.org/10.5194/acp-15-12345-2015>, 2015.
- Xu, W., Wu, Q. H., Liu, X. J., Tang, A. H., Dore, A. J., and Heal, M. R.: Characteristics of ammonia, acid gases, and PM_{2.5} for three typical land-use types in the North China Plain, *Environ. Sci. Pollut. Res.*, 23, 1158–1172, <https://doi.org/10.1007/s11356-015-5648-3>, 2016.
- Xu, W., Song, W., Zhang, Y., Liu, X., Zhang, L., Zhao, Y., Liu, D., Tang, A., Yang, D., Wang, D., Wen, Z., Pan, Y., Fowler, D., Collett Jr., J. L., Erisman, J. W., Goulding, K., Li, Y., and Zhang, F.: Air quality improvement in a megacity: implications from 2015 Beijing Parade Blue pollution control actions, *Atmos. Chem. Phys.*, 17, 31–46, <https://doi.org/10.5194/acp-17-31-2017>, 2017.
- Xu, W., Zhao, Y. H., Liu, X. J., Dore, A. J., Zhang, L., Liu, L., and Cheng, M.: Atmospheric nitrogen deposition in the Yangtze River basin: Spatial pattern and source attribution, *Environ. Pollut.*, 232, 546–555, <https://doi.org/10.1016/j.envpol.2017.09.086>, 2018.
- Yang, F., Tan, J., Zhao, Q., Du, Z., He, K., Ma, Y., Duan, F., Chen, G., and Zhao, Q.: Characteristics of PM_{2.5} speciation in representative megacities and across China, *Atmos. Chem. Phys.*, 11, 5207–5219, <https://doi.org/10.5194/acp-11-5207-2011>, 2011.
- Yang, Y. H., Li, P., He, H. L., Zhao, X., Datta, A., Ma, W. H., Zhang, Y., Liu, X. J., Han, W. X., Wilson, M. C., and Fang, J. Y.: Long-term changes in soil pH across major forest ecosystems in China, *Geophys. Res. Lett.*, 42, 933–940, <https://doi.org/10.1002/2014GL062575>, 2015.
- Zhang, L., Chen, Y. F., Zhao, Y. H., Henze, D. K., Zhu, L. Y., Song, Y., Paulot, F., Liu, X. J., Pan, Y. P., and Huang, B. X.: Agricultural ammonia emissions in China: reconciling bottom-up and top-down estimates, *Atmos. Chem. Phys.*, 18, 339–355, <https://doi.org/10.5194/acp-18-339-2018>, 2018.
- Zhang, L. M., Gong, S. L., Padro, J., and Barrie, L.: A size-segregated particle dry deposition scheme for an atmospheric aerosol module, *Atmos. Environ.*, 35, 549–560, [https://doi.org/10.1016/s1352-2310\(00\)00326-5](https://doi.org/10.1016/s1352-2310(00)00326-5), 2001.
- Zhang, Q., Duan, F. K., He, K. B., Ma, Y. L., Li, H. Y., Kimoto, T., and Zheng, A. H.: Organic nitrogen in PM_{2.5} in Beijing, *Front. Environ. Sci. Eng.*, 9, 1004–1014, <https://doi.org/10.1007/s11783-015-0799-5>, 2015.
- Zhang, X. M., Wu, Y. Y., Liu, X. J., Reis, S., Jin, J. X., Dragosits, U., Damme, Van M., Clarisse, L., Whitburn, S., and Coheur, P. F.: Ammonia emissions may be substantially underestimated in China, *Environ. Sci. Technol.*, 51, 12089–12096, <https://doi.org/10.1021/acs.est.7b02171>, 2017.
- Zhao, Y., Nielsen, C. P., Lei, Y., McElroy, M. B., and Hao, J.: Quantifying the uncertainties of a bottom-up emission inventory of anthropogenic atmospheric pollutants in China, *Atmos. Chem. Phys.*, 11, 2295–2308, <https://doi.org/10.5194/acp-11-2295-2011>, 2011.
- Zhao, Y., Zhang, L., Pan, Y., Wang, Y., Paulot, F., and Henze, D. K.: Atmospheric nitrogen deposition to the northwestern Pacific: seasonal variation and source attribution, *Atmos. Chem. Phys.*, 15, 10905–10924, <https://doi.org/10.5194/acp-15-10905-2015>, 2015.
- Zhao, Y., Zhang, L., Chen, Y. F., Liu, X. J., Xu, W., Pan, Y. P., and Duan, L.: Atmospheric nitrogen deposition to China: a model analysis on nitrogen budget and critical load exceedance, *Atmos. Environ.*, 153, 32–40, <https://doi.org/10.1016/j.atmosenv.2017.01.018>, 2017.
- Zhu, J. X., He, N. P., Wang, Q. F., Yan, G. F., Wen, D., Yu, G. R., and Jia, Y. L.: The composition, spatial patterns, and influencing factors of atmospheric wet nitrogen deposition in Chinese terrestrial ecosystems, *Sci. Total Environ.*, 511, 777–785, <https://doi.org/10.1016/j.scitotenv.2014.12.038>, 2015.